iScience

CellPress
OPEN ACCESS

Article

Cell non-autonomous control of autophagy and metabolism by glial cells

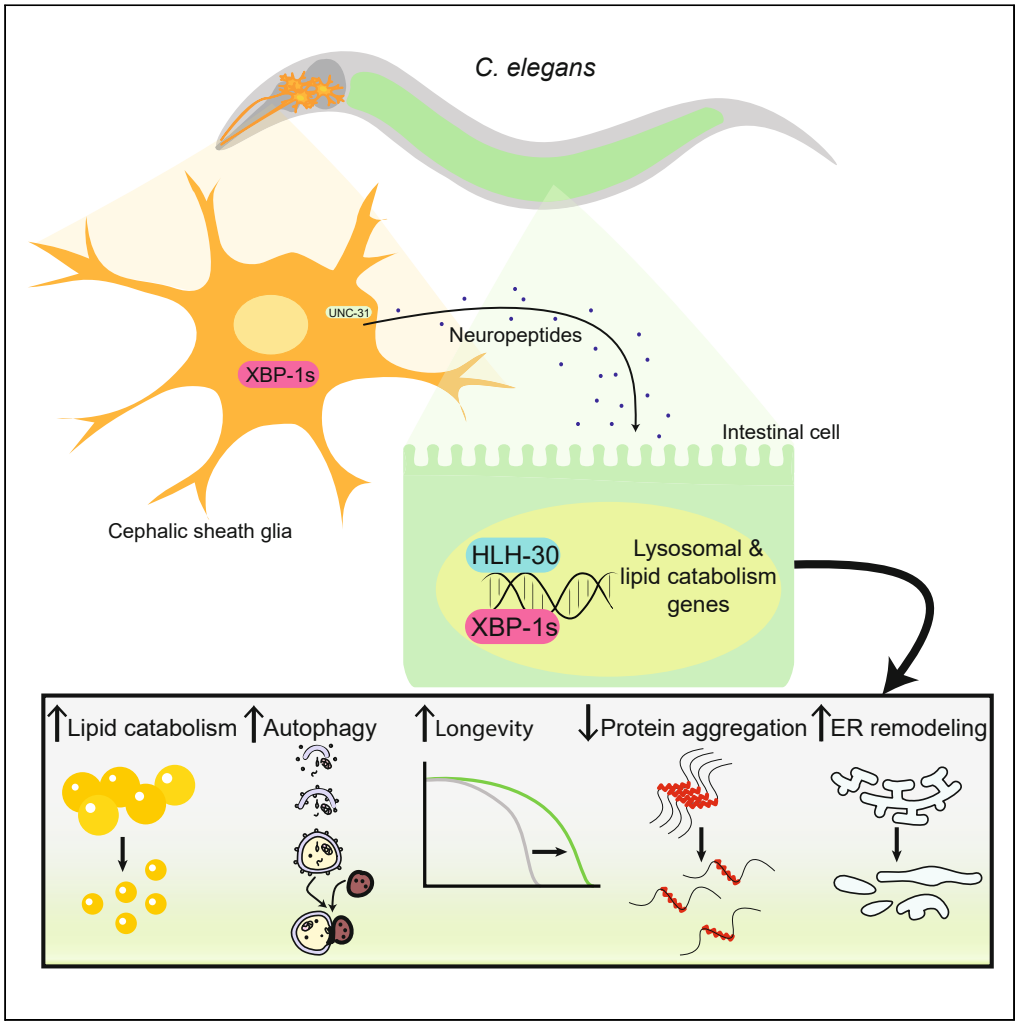

Melissa G. Metcalf, Samira Monshietehadi, Arushi Sahay, ..., Amelia Farinas, Melissa Sanchez, Andrew Dillin

dillin@berkeley.edu

Highlights

Glial XBP-1s reduces peripheral lipids, boosts autophagy, and changes ER structure

Glial XBP-1s regulates the activation of HLH-30 in the intestine

Lipid depletion and lifespan extension phenotypes are dependent on *hlh-30*

Macroautophagy genes are required for longevity and altered ER structure

Metcalf et al., iScience *27*, 109354
April 19, 2024
https://doi.org/10.1016/j.isci.2024.109354

iScience

CellPress
OPEN ACCESS

Article

Cell non-autonomous control of autophagy and metabolism by glial cells

Melissa G. Metcalf,[1,2] Samira Monshietehadi,[1,2] Arushi Sahay,[1,2] Jenni Durieux,[1,2] Ashley E. Frakes,[1,2] Martina Velichkovska,[1,2] Cesar Mena,[1,2] Amelia Farinas,[1,2] Melissa Sanchez,[1,2] and Andrew Dillin[1,2,3,*]

SUMMARY

Glia are the protectors of the nervous system, providing neurons with support and protection from cytotoxic insults. We previously discovered that four astrocyte-like glia can regulate organismal proteostasis and longevity in *C. elegans*. Expression of the UPR^{ER} transcription factor, XBP-1s, in these glia increases stress resistance, and longevity, and activates the UPR^{ER} in intestinal cells via neuropeptides. Autophagy, a key regulator of metabolism and aging, has been described as a cell autonomous process. Surprisingly, we find that glial XBP-1s enhances proteostasis and longevity by cell non-autonomously reprogramming organismal lipid metabolism and activating autophagy. Glial XBP-1s regulates the activation of another transcription factor, HLH-30/TFEB, in the intestine. HLH-30 activates intestinal autophagy, increases intestinal lipid catabolism, and upregulates a robust transcriptional program. Our study reveals a novel role for glia in regulating peripheral lipid metabolism, autophagy, and organellar health through peripheral activation of HLH-30 and autophagy.

INTRODUCTION

The central nervous system senses and processes internal and afferent signals, which convey information about nutrient status and stress within an organism. The ability of the brain to accurately detect and correctly respond to these signals is essential for the survival of all animals. Both glial cells and glia-neuronal contact sites are hubs for integrating metabolic cues.[1] Signals sent from the nervous system, after detecting changes in internal or external environments, have been shown to modulate lifespan while also regulating protein homeostasis (proteostasis) and stress resistance.[2–6] As an organism ages, the ability of a cell to detect and respond to cellular and organismal stressors declines. Thus, the ability of the nervous system to detect and respond to signals from the environment and inter-organ communication can shape the progression of the aging process and the onset of age-associated diseases.[7,8]

A cell employs numerous mechanisms to respond to cellular insults and maintain proteostasis through the coordinated action of distinct stress response pathways in their organelles and cellular compartments.[9] A key stress response pathway is found in the endoplasmic reticulum (ER), an organelle that has a central role in lipid and protein biosynthesis, being the site of production of all the transmembrane proteins and lipids for the majority of a cell's organelles.[10] Increased protein or lipid demands within a cell disrupt the function of the ER and increase ER stress, triggering the unfolded protein response of the ER (UPR^{ER}) to restore cellular homeostasis.[11] The IRE-1 branch of the UPR^{ER} detects unfolded proteins in the ER lumen and lipid perturbations in the ER membrane, leading to the regulated splicing of the mRNA encoding the transcription factor XBP-1.[12–17] Spliced XBP-1, XBP-1s, is subsequently translated, leading to the regulation of transcriptional targets to reduce ER stress by repressing protein translation, regulating lipid synthesis, inducing protein chaperone expression, and eliminating misfolded and damaging proteins.[18–20]

UPR^{ER} activation in the nervous system can be non-autonomously communicated to other tissues to regulate organismal stress resistance and longevity.[3,4] Pan-neuronal activation of the UPR^{ER} leads to organismal effects on lysosomal and lipid metabolism via neurotransmitter signaling in the roundworm *Caenorhabditis elegans*.[21–25] *C. elegans* has a simple nervous system, with 302 neurons and 56 glial cells encompassing close to one-third of the total cells in the organism.[26] Of the 56 glial cells, the four glial cells of the cephalic sheath (CEPsh) are positioned around the brain of *C. elegans*, the "nerve ring", with their anterior processes forming a sensory organ at the mouth of the organism.[26] CEPsh glia have numerous functions that parallel mammalian glial cell types, including regulating the interface between peripheral organs and the nervous system, providing trophic support, and acting as neuronal and glial progenitors.[26–30] Over-expression of a UPR^{ER} transcription factor, XBP-1s, in CEPsh glia leads to lifespan extension and ER stress resistance through induction of the UPR^{ER} in distal intestinal cells through the release of dense core vesicles (DCV) and neuropeptides.[2] These findings indicate that this subset of glial cells can regulate

[1]Department of Molecular and Cell Biology, University of California, Berkeley, Berkeley, CA 94720, USA
[2]Howard Hughes Medical Institute, University of California, Berkeley, Berkeley, CA 94720, USA
[3]Lead contact
*Correspondence: dillin@berkeley.edu
https://doi.org/10.1016/j.isci.2024.109354

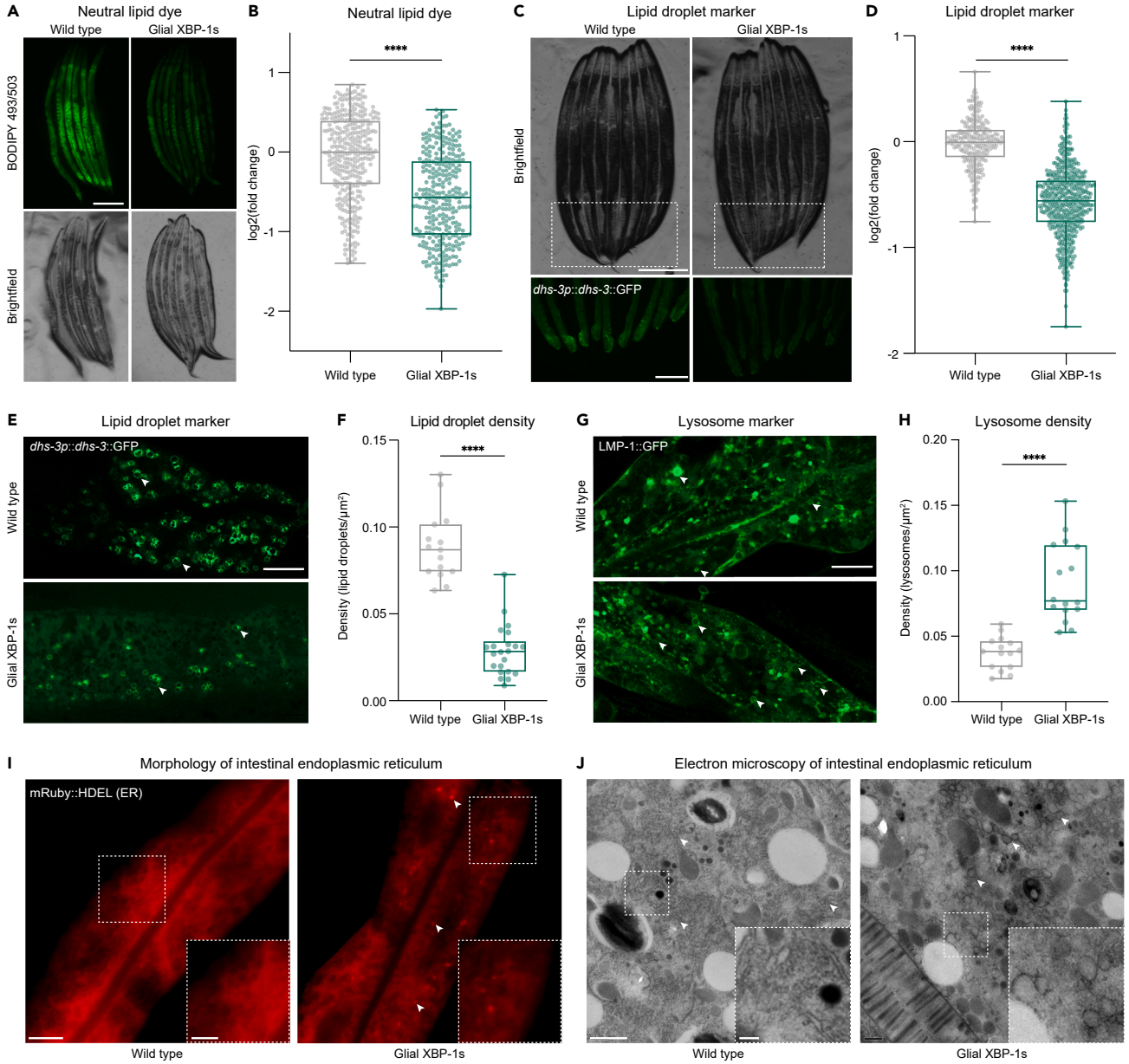

Figure 1. Expression of XBP-1s in CEPsh glia modulates peripheral lipid metabolism and ER remodeling in *C elegans*

(A) Fluorescent light micrographs of wild-type (N2) and glial XBP-1s animals stained with BODIPY 493/503 dye and imaged at day 2 of adulthood. Scale bar, 250 μm.

(B) Whole animal fluorescence intensity quantification of BODIPY 493/503 dye in day 2 adults in wild-type (gray) and glial XBP-1s animals (green) using COPAS BioSorter. $p < 0.0001$ (****), using the non-parametric Mann-Whitney test. Plots are representative of three biological replicates, n = 362 (wild type) and n = 302 (glial XBP-1s). Results were normalized to the mean fluorescent intensity of wild-type animals. Each dot represents one animal, and the boxplot shows the median (horizontal line), the first and third quartiles (box), and the smallest and largest data points (whiskers).

(C) Fluorescent light micrographs of wild-type and glial XBP-1s animals of intestinal lipid droplets (*dhs-3*p::*dhs-3*::GFP) imaged at day 2 of adulthood. Scale bar, 250 μm.

(D) Whole animal fluorescence intensity quantification of intestinal *dhs-3*p::*dhs-3*::GFP lipid droplet marker in wild-type (gray) and glial XBP-1s animals (green) using COPAS BioSorter. $p < 0.0001$ (****), using the non-parametric Mann-Whitney test. Plots are representative of three biological replicates, n = 254 (wild type) and n = 532 (glial XBP-1s). Results were normalized to the mean fluorescent intensity of wild-type animals transgenic for *dhs-3*p::*dhs-3*::GFP.

(E) Representative Airyscan micrographs of *dhs-3*p::*dhs-3*::GFP labeled lipid droplets from anterior intestines of day 2 wild-type and glial XBP-1s adult animals. Arrowheads point at lipid droplets: scale bar, 10 μm.

(F) Quantification of intestinal *dhs-3*p::*dhs-3*::GFP labeled lipid droplets in wild-type (gray) and glial XBP-1s (green) animals. Lipid droplets were counted from three independent replicates using ImageJ and expressed as density. Density was determined by dividing the number of lipid droplets by the total area

systemic proteostasis, inter-organ communication, and organismal aging through neuropeptide signaling. However, the downstream mechanisms regulating these phenotypes remain unknown.

Here, we find that ectopic expression of constitutively active XBP-1s in four CEPsh glial cells initiates a robust metabolic program, leading to lipid depletion and ER remodeling peripherally. Cell non-autonomous signaling from CEPsh glia activates intestinal HLH-30, a transcription factor important for lysosomal and autophagy homeostasis.[31] Interestingly, HLH-30 is required for the lipid depletion, lifespan extension, and increased proteostasis of glial XBP-1s animals. In parallel to HLH-30 activation in the periphery, glial XBP-1s animals have activated autophagy in intestinal tissue. Autophagy is required for the extension of longevity and increased ER remodeling in the intestine of glial XBP-1s animals. Finally, glial XBP-1s signaling to activate HLH-30 in the periphery requires DCV release. Taken together, we find that cell non-autonomous signaling from XBP-1s expressing CEPsh glia activates a peripheral metabolic program required for the beneficial impacts on organismal proteostasis, organellar health, and longevity.

RESULTS

Glial XBP-1s animals have reduced lipid content, droplet number, and increased lysosomes in their periphery

The UPR^{ER} and XBP-1 have been shown to regulate lipid metabolism, and changes in lipid metabolism regulate lifespan.[32–34] To determine if the long-lived and stress-resistant animals overexpressing the coding sequence of *xbp-1s* in CEPsh glia (glial XBP-1s) altered peripheral lipid metabolism, we measured whole-body total neutral lipid content via BODIPY 493/503 staining. We found that glial XBP-1s animals had significantly reduced staining of total neutral lipids compared to wild-type animals, suggesting that glial UPR^{ER} activation leads to reduced peripheral lipid stores (Figures 1A and 1B), which is not due to differences in background autofluorescence (Figure S1A). When comparing neutral lipid content to animals with known fat storage defects, *eat-2(e1372)* and *daf-7(ad1116)*, show increased and decreased BODIPY 493/503, respectively (Figure S1B).[35]

Lipid droplets are a conserved organelle for fat storage and the main storage site of intestinal lipids in *C. elegans*. We hypothesized that lipid droplet content may be reduced in glial XBP-1s animals.[36] We visualized lipid droplets using an intestinally-expressed green fluorescent protein (GFP)-tagged construct of a short-chain dehydrogenase, DHS-3, which localizes to lipid droplet membranes in *C. elegans*.[37] Using this marker, we found that glial XBP-1s animals had reduced fluorescence intensity of the DHS-3:GFP lipid droplet marker when compared to wild-type animals (Figures 1C and 1D) and that this decrease was not due to differences in basal autofluorescence (Figure S1C). Further, we observed a decrease in lipid droplet density, determined by the number of lipid droplets per area of the intestine imaged, in the intestines of glial XBP-1s animals compared to wild-type animals (Figures 1E and 1F). These data point to the intestine of glial XBP-1s animals, the same organ that receives a signal to activate the UPR^{ER}, having reduced lipid content.

We hypothesized that the reduced lipid content in glial XBP-1s animals may be due to increased lipid catabolism by lysosomes. Lysosomes act as cellular regulators of energy metabolism, functioning as both catabolic recycling centers within a cell and metabolic signaling and sensing hubs that govern cell growth decisions.[38,39] We investigated if there was an increase in lysosome content in the intestine of glial XBP-1s animals, which may be indicative of increased lipid catabolism.[40] Lysosome density was measured using a GFP-fusion protein of the *C. elegans* homolog of the lysosomal surface protein LAMP1, *lmp-1* (Figure 1G). Using this marker, we found that glial XBP-1s animals had significantly higher lysosome density in their intestine when compared to wild-type animals (Figure 1H). To confirm that the decrease in lipid content and increase in lysosome numbers was not due to a decrease in food intake, we compared the feeding rates of glial XPB-1s animals to control. Glial XBP-1s animals have similar pumping rates to wild-type animals, indicating that they are consuming comparable amounts of their bacterial food source (Figure S1D).[41] This increase in lysosomal number within the intestine of glial XBP-1s animals is indicative of an increase in organismal lipid catabolic and proteostatic activity.

Glial XBP-1s animals have altered ER morphology and function in distal tissues

As the central hub for membrane biogenesis and the production of the majority of membrane lipids, the ER is particularly sensitive to changes in lipid content, which can drastically change its structure and function.[42,43] Activation of the UPR^{ER} increases both the size of the ER and its folding capacity to reestablish homeostasis within the organelle.[43–46] To test if glial UPR^{ER} activation affected peripheral ER morphology, we visualized the intestinal ER using a fusion protein, *vha-6p*::ERss:mRuby:HDEL, that localizes to the ER lumen through a heat shock protein 4 (HSP-4) signal sequence, is retained in the ER through a C-terminal HDEL sequence, and expresses a red fluorescent protein, mRuby.

Figure 1. *Continued*

expressing *dhs-3*p::*dhs-3*::GFP in each respective image. N = 15 (wild type) and N = 22 (glial XBP-1s). $p < 0.0001$ (****), using the non-parametric Mann-Whitney test.

(G) Representative Airyscan micrographs of *lmp-1*::GFP labeled lysosomes in the anterior intestine of day 2 adults in both wild-type and glial XBP-1s animals. Arrowheads point at lysosomes: scale bar, 10 μm.

(H) Quantification of intestinal *lmp-1*::GFP labeled lysosomes in wild-type (gray) and glial XBP-1s (green) animals. Lysosomes were counted from three independent replicates using ImageJ and expressed as density. Density was determined by dividing the number of lysosomes by the total area that expressed *lmp-1*::GFP in each respective image. N = 15 (wild type) and N = 16 (glial XBP-1s). $p < 0.0001$ (****), using the non-parametric Mann-Whitney test.

(I) Representative confocal micrographs of intestinal ER morphology (*vha-6p*::ERss:mRuby:HDEL, ERss = *hsp- 4* ER signal sequence), wild-type and glial XBP-1s animals were imaged at day 2 of adulthood. Arrowheads mark ER puncta. Scale bar, 10 μm. Scale bar of inset, 5 μm.

(J) Electron micrographs of intestine from wild-type and glial XBP-1s animals at day 2 of adulthood. Imaging was replicated in triplicate, for a total of 15–20 animals being imaged per condition. Arrowheads mark rough endoplasmic reticulum. Scale bar, 1μm. Scale bar of inset, 0.2 μm.

Interestingly, glial XBP-1s animals form puncta of mRuby:HDEL labeled ER that are not seen in wild-type animals (Figure 1I). Additionally, we found that glial XBP-1s animals had an increase in intestinal secretion of secretory proteins, visualized using VIT-2:GFP (Figure S1E). VIT-2:GFP is a fluorescent fusion protein of vitellogenin, a yolk protein that is produced in the intestinal ER of *C. elegans*, secreted, and then endocytosed by developing eggs.[47] The level of VIT-2:GFP fluorescence in egg cells is used as a proxy for ER function in the intestine of *C. elegans*.[25] To better understand the nature of these changes in the intestinal ER of glial XBP-1s animals, we performed high-magnification transmission electron microscopy (TEM) (Figure 1J). We identified changes in rough ER morphology in glial XBP-1s animals, where rough ER formed circular-like structures compared to the reticulated ER structure in wild-type animals (Figure S1F). Taken together, these results demonstrate that glial XBP-1s animals have changes in ER morphology within their intestines, indicating expansion of the ER, as well as increased secretion of secretory proteins.

HLH-30/TFEB is required for glial XBP-1s lifespan extension

The changes in storage fat levels, lipid droplet content, and increased lysosome number suggest that a master regulator of metabolism is activated in the periphery of these glial XBP-1s animals. Because these metabolic phenotypes are predictors of longevity of the glial XBP-1s animals, we asked which, if any, of the known master regulators of metabolic function might be required for the glial XBP-1s animals' increased longevity. We found that the lifespan extension of glial XBP-1s animals was not dependent on key regulators of metabolism: *daf-16* (FOXO), *aak-1* and *aak-2* (AMPK), or *pha-4* (FOXA) (Figures 2A–2D).[48–52] Surprisingly, glial XBP-1s animals had significantly upregulated levels of fluorescently tagged DAF-16 protein, DAF-16:GFP; however, nuclear localization of this transcription factor was not observed, suggesting that DAF-16 is not functioning to increase its target genes' transcription (Figures S2A and S2B). HLH-30, the *C. elegans* ortholog of the mammalian transcription factor EB (TFEB), a master regulator of lysosomal biogenesis, autophagy, and lipid catabolism, was found to be required for glial XBP-1s lifespan extension.[31,53–55] Knockdown of *hlh-30* via RNAi treatment suppressed the lifespan extension in glial XBP-1s animals (Figure 2E). In parallel, we found that loss of *hlh-30*, via a loss-of-function mutation *hlh-30(tm1978)*, suppressed the lifespan extension of glial XBP-1s animals (Figure 2F). These data point to a role for the transcription factor HLH-30 in mediating longevity in glial XBP-1s animals, and not other known regulators of metabolism.

HLH-30/TFEB is activated cell non-autonomously in peripheral tissue of glial XBP-1s animals via DCV release

HLH-30 is activated under times of stress to meet the metabolic needs of an organism with the cellular resources available. When HLH-30 is inactive, it is sequestered in the cytosol via scaffolding proteins, and upon activation via phosphorylation, HLH-30 moves from the cytoplasm into the nucleus. We used a fluorescent fusion protein, HLH-30:GFP, to determine levels of nuclear localization of HLH-30:GFP in the intestine of glial XBP-1s animals as a proxy for HLH-30 activation.[31] We observed HLH-30:GFP to be enriched prominently in the nuclei of intestinal cells in adult glial XBP-1s animals (Figures 3A–3C). These data indicate that HLH-30 is activated peripherally in the intestine when *xbp-1s* is constitutively active in CEPsh glia.

We next asked if the intestinal nuclear localization of HLH-30 in glial XBP-1s animals is activated in a cell non-autonomous manner or if it is simply a byproduct of UPR^{ER} activation in the periphery. It has previously been shown that glial XBP-1s animals transmit a signal, via release DCVs release of neuropeptides that is detected by the intestine to activate the UPR^{ER}.[2] We observed a reversal of the HLH-30:GFP intestinal nuclear localization back to the cytoplasmic localization found in wild-type animals when visualizing HLH-30:GFP in glial XBP-1s animals with a loss-of-function mutation that disrupts DCV exocytosis, *unc-31(e928)* (Figure 3D). Importantly, the *unc-31(e928)* mutation did not alter HLH-30 localization, nor did it block the ability of HLH-30 to transit to the nucleus when animals were treated with heat stress, a known activator of HLH-30 (Figure S3A).[56]

Glial and neuronal signaling of XBP-1s activation are distinct from each other. Glial XBP-1s animals do not signal to the periphery to activate the UPR^{ER} using neurotransmitters or small clear vesicles (SCV), as in the neuronal XBP-1s paradigm.[2,3,22,23] To test if peripheral HLH-30 activation is specific to DCV signaling in glial XBP-1s animals, we blocked SCV release via an *unc-13* loss-of-function mutation, *unc-13(e51)*, and found that the loss of SCV release did not suppress the activation of HLH-30 in the periphery (Figure S3B). Taken together, glial XBP-1s animals transmit a distinct signal through DCV release which is detected by the intestine and leads to increased nuclear localization of HLH-30.

As a final test, if HLH-30 localization was a byproduct of ER stress activation in glial XBP-1s animals, HLH-30:GFP animals were treated with the drug tunicamycin, which induces ER stress via inhibiting protein glycosylation, thus blocking protein folding and transit through the ER. Tunicamycin-induced ER stress does not affect the nuclear localization of HLH-30 (Figure 3E). Furthermore, animals treated with tunicamycin do not activate the transcription of HLH-30 autophagy and lysosomal-related target genes (Figure S3C).[31] Interestingly, animals lacking functional XBP-1, via an *xbp-1(tm2492)* deletion had suppressed nuclear localization of HLH-30 (Figure S3D). Taken together, glial XBP-1s animals transmit a distinct signal to activate HLH-30 in their periphery that cannot be accomplished by cell autonomous ER stress, the signal must come in part from glial cells.

Surprised to find that HLH-30 could be activated cell non-autonomously from glial cells by XBP-1s, we asked whether HLH-30 could activate itself cell non-autonomously if activated in these same glial cells. Ectopic overexpression of *hlh-30* across the entire animal has been shown to increase lifespan and induce HLH-30 target genes.[31] Using the same *hlh-30* construct, but now restricted to expression in the four CEPsh glia, we did not observe nuclear localization of HLH-30 in peripheral cells (Figure S3E), nor do we find increased lifespan of these animals (Figure S3F). These data indicate that the expression *of xbp-1s* in CEPsh glia can uniquely activate HLH-30 in the periphery and extend lifespan, which cannot be simply achieved by *hlh-30* expression in these cells.

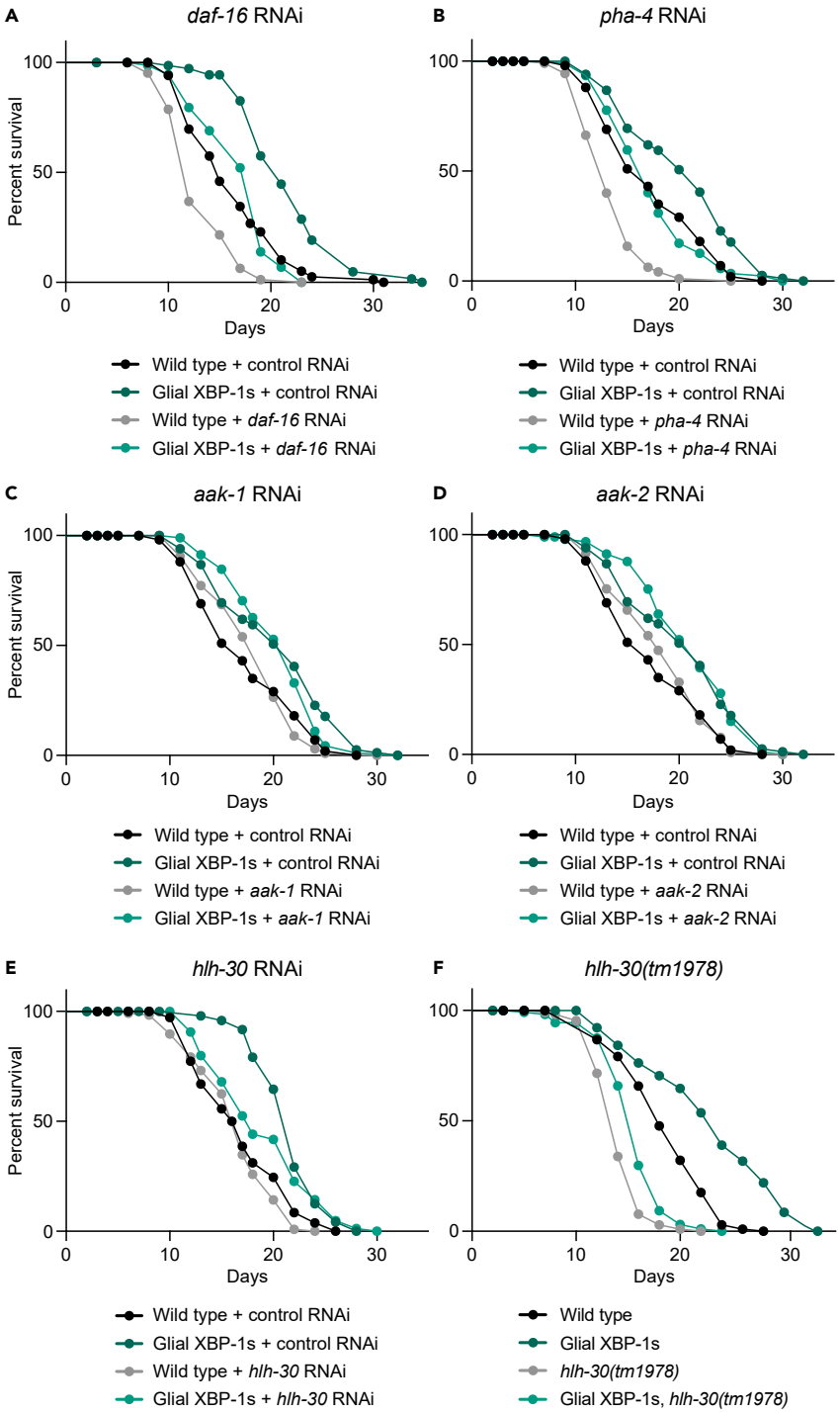

Figure 2. Lifespan screen of key metabolic regulators reveals HLH-30 requirement for longevity of glial XBP-1s animals

(A–E) Survival of wild-type (N2) and glial XBP-1s animals on control (HT115 *E. coli* expressing empty vector), *daf-16* (A), *aak-1* (B), *aak-2* (C), *pha-4* (D), and *hlh-30* (E) RNAi from L4 at 20°C. Lifespan is representative of three replicates. Graphs were plotted as Kaplan-Meier survival curves and p values were calculated by Mantel-Cox log rank test. See Table S1 for lifespan statistics.

(F) Survival of wild-type and glial XBP-1s animals on control RNAi at 20°C, with and without *hlh-30(tm1978)* mutation. The graph was plotted as Kaplan-Meier survival curves and p values were calculated by the Mantel-Cox log rank test. See Table S1 for lifespan statistics.

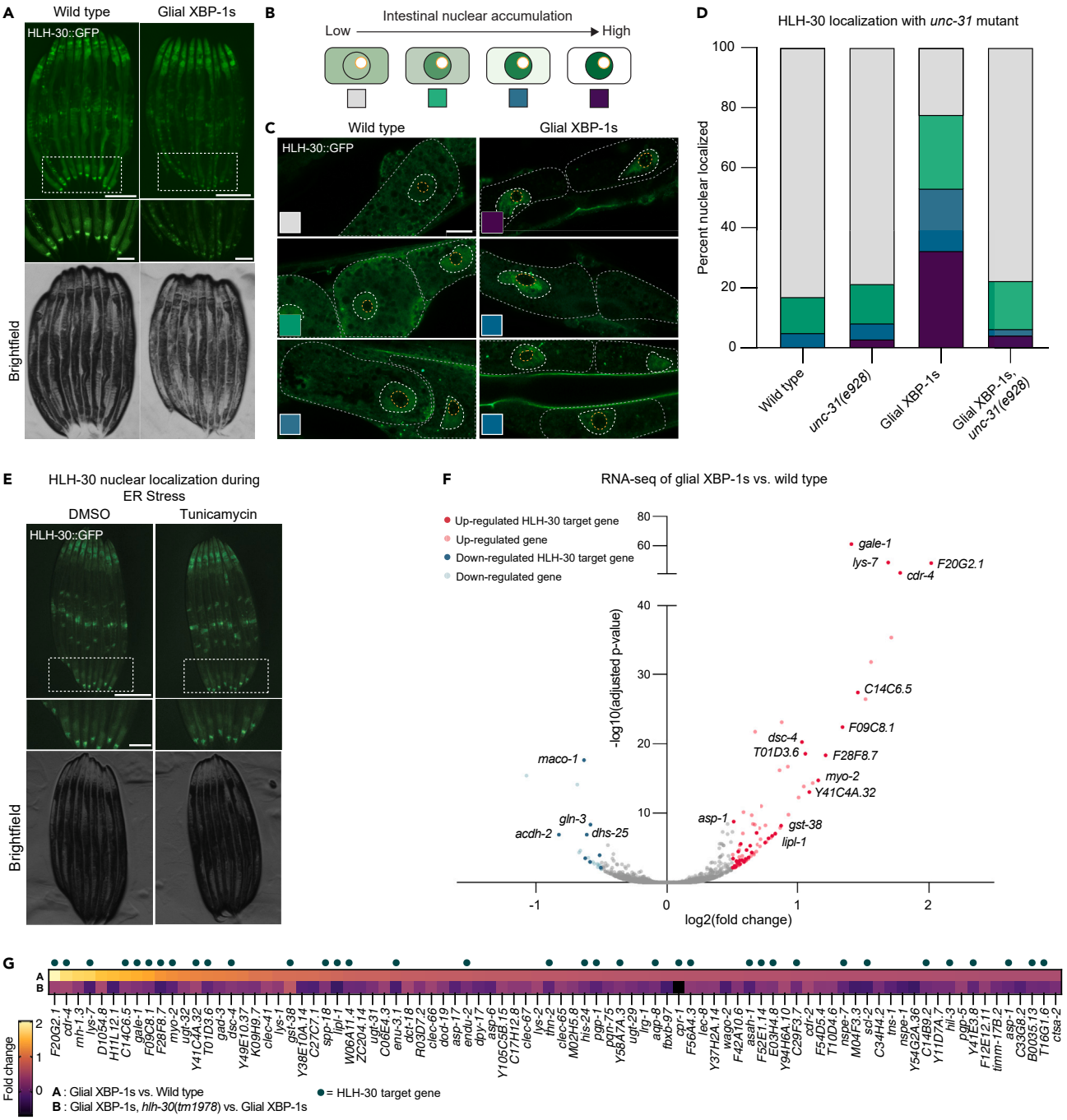

Figure 3. Glial XBP-1s cell non-autonomously activates intestinal HLH-30 which transcriptionally regulates genes involved in lipid catabolism and lysosomal biogenesis

(A) Fluorescent light micrographs of wild-type and glial XBP-1s animals transgenic for fluorescently tagged HLH-30 (HLH-30:GFP) grown on OP50 and imaged at day 2 of adulthood. HLH-30 translocates to the nucleus in glial XBP-1s animals. The inset shows posterior intestine. Scale bar, 250μm. Scale bar of inset, 100μm.

(B) Schematic showing how HLH-30:GFP nuclear localization was scored. Categories include no nuclear enrichment (gray), weak nuclear enrichment (green), medium nuclear enrichment (blue), and strong nuclear enrichment (purple). Yellow circle indicates nucleolus, which transcription factors are excluded from.

(C) Representative Airyscan micrographs of posterior intestinal cells of wild-type and glial XBP-1s animals transgenic for HLH-30:GFP grown on OP50 and imaged at day 2 of adulthood. Colored inset squares are representative of the scoring categories from (B). Scale bar, 10μm. Intestinal cells are outlined with a dashed gray line, intestinal nuclei are outlined with a dashed white line and intestinal nucleoli are outlined with a dashed yellow line.

Figure 3. *Continued*

(D) Nuclear translocation of HLH-30:GFP in anterior intestinal cells of day 2 adult wild-type and glial XBP-1s animals with and without the loss-of-function *unc-31* mutant, *unc-31(e928)*, N > 40 animals per condition from three independent replicates. Statistics done by Chi-squared test for independence with adjusted residual and Bonferroni correction, statistics shown in Table S4.

(E) Representative fluorescent micrograph of wild-type animals transgenic for HLH-30:GFP treated with either DMSO or tunicamycin. Inset shows posterior intestine. Scale bar, 250 μM. Scale bar of inset, 100 μM. Image is representative of two independent replicates, in n > 20 no animals showed nuclear localization.

(F) Volcano plot demonstrating magnitude (log2[fold change]) and significance (-log10[adjusted p value]) of changes in gene expression from whole-animal RNA sequencing of glial XBP-1s versus wild-type animals at day 2 of adulthood. Differentially expressed genes (DEGs) shown in red (upregulated, adjusted p value <0.05 and log2[fold change] > 0.5, n = 86) and blue (downregulated, adjusted p value<0.05 and log2[fold change] < 0.5, n = 22). Labeled genes and DEGs with dark red (upregulated DEGs) and dark blue (down-regulated DEGs) dots correspond to HLH-30 targets which are labeled with their corresponding gene.

(G) Comparison of log2(fold change) of the 86 upregulated DEGs in glial XBP-1s animals compared to wild-type animals (top) compared to the log2(fold change) of these genes in glial XBP-1s animals with a loss-of-function *hlh-30* mutation, *hlh-30(tm1978)*, compared to glial XBP-1s animals alone (bottom). log2(fold change) is color-coded via a heatmap from warm (upregulated) to cool (downregulated). Green dots above the heatmap represent HLH-30 target genes. Statistics shown in Table S5.

HLH-30 transcriptionally regulates a high proportion of upregulated genes in glial XBP-1s animals

Finding that HLH-30 is oriented in a unique position to specifically regulate the downstream effects of glial XBP-1s-induced longevity, we sought to better understand how HLH-30 could execute these downstream functions in such a distinctive manner. To do so, we asked if the transcriptional and phenotypic changes we observed in the peripheral cells were mediated, in part or completely, by HLH-30.

RNA sequencing revealed substantial gene expression changes in glial XBP-1s animals when compared to wild-type animals, with over a third of upregulated genes being HLH-30 transcriptional targets. To identify HLH-30 target genes that are significantly changed in the glial XBP-1s animals, we generated a list of genes that were previously reported to be HLH-30 targets and had HLH-30 binding sites in the immediate upstream region from the start codon.[57–59] Of the 86 upregulated genes ($p < 0.05$ and log2[fold change] > 0.5) in glial XBP-1s animals, 36 are HLH-30 targets (Figures 3F; Table S1). These genes have roles in lysosomal lipid and protein catabolism, antioxidant production, immune response, and the UPR^{ER} (Table S2). Additionally, we found that that all glial XBP-1s-upregulated genes were at least partly suppressed by a loss-of-function mutation in *hlh-30*, and *hlh-30(tm1978)* (Figure 3G and S3G). These data indicate that constitutive activation of *xbp-1s* in the four CEPsh glia in *C. elegans* leads to activation of a peripheral metabolic transcriptional program partly through the activation of HLH-30.

Glial XBP-1s promotes peripheral autophagy activation

HLH-30 serves critical functions in autophagy through its regulation of numerous autophagy and lysosomal-related genes. Because we observed activated HLH-30 in the periphery of glial XBP-1s animals, we hypothesized that there would be an increase in autophagy activation in their distal intestinal cells. First, we asked if glial XBP-1s animals had changes in autophagosome (AP) and autolysosome (AL) content. The number of APs and ALs was determined using the dual-fluorescent reporter of LGG-1, the *C. elegans* ortholog of Atg8, mCherry:GFP::LGG-1.[60] LGG-1 is cleaved during AP formation, conjugated to phosphatidylethanolamine, and inserted into the AP membrane. The tandem mCherry/GFP reporter allows for the determination of APs versus ALs, due to GFP fluorescence quenching in the highly acidic lysosomal environment.[60] Thus, yellow puncta (co-labeled with GFP/mCherry (pseudo-labeled in magenta) monitor APs, and red puncta monitor the level of ALs within a cell.

Interestingly, the density of APs remains similar at both day 2 and day 5 of adulthood in wild-type and glial XBP-1s animals (Figures 4A and 4B). We see an increase in the density of ALs in glial XBP-1s relative to wild-type animals at both day 2 and day 5 of adulthood (Figures 4A and 4C). Interestingly, we find that the number of APs and ALs in glial XBP-1s animals is dependent on *hlh-30* (Figures S4A and S4B). To corroborate the *in vivo* analysis of autophagy induction, we asked if glial XBP-1s animals had an increase in autophagy and lysosomal genes that are known targets of HLH-30.[31] Indeed, we found a significant increase in the transcripts of *hlh-30*, autophagy-related, and lysosomal-related genes via qPCR (Figure S4C). These data indicate that expression of XBP-1s in CEPsh glia cell non-autonomously activates autophagy peripherally in their intestines over age.

While it is of great interest to determine if the activation of peripheral autophagy is dependent on DCV release, using the *unc-31(e928)* mutant to probe this provides some challenges. First, mutations in *unc-31* are known to disrupt neuropeptide signaling, including insulin-like signaling, which in turn can activate autophagy in these animals.[61,62] We confirmed this probing for targets of HLH-30 in *unc-31(e928)* mutant animals and found that there was significant upregulation of these genes in *unc-31(e928)* mutant animals (Figure S4E).

HLH-30/TFEB is required for the reduction in lipid droplets and intestinal protein aggregates in glial XBP-1s animals

Since HLH-30 has transcriptional control over genes involved in lysosome biogenesis and lipid catabolism, we asked if the decreased lipid droplet content in the intestine of glial XBP-1s animals is dependent on *hlh-30*. We found that *hlh-30* is required for the reduction of lipid droplets in glial XBP-1s animals (Figure 4D). When *hlh-30* is knocked down in glial XBP-1s animals the density of intestinal lipid droplets returns to wild-type levels (Figure 4E). These data point to a requirement for *hlh-30* in the reduction of lipid stores in the intestines of glial XBP-1s animals.

HLH-30 has also been shown to be necessary for protection against proteotoxicity in *C. elegans* overexpressing *xbp-1s* pan-neuronally.[21] It has also been shown that expression of *xbp-1s* in CEPsh glia leads to a significant reduction in aggregation of yellow fluorescent protein (YFP)-tagged polyglutamine (polyQ) repeat expansion protein in the intestine.[2] Proteins with polyQ expansions are implicated in

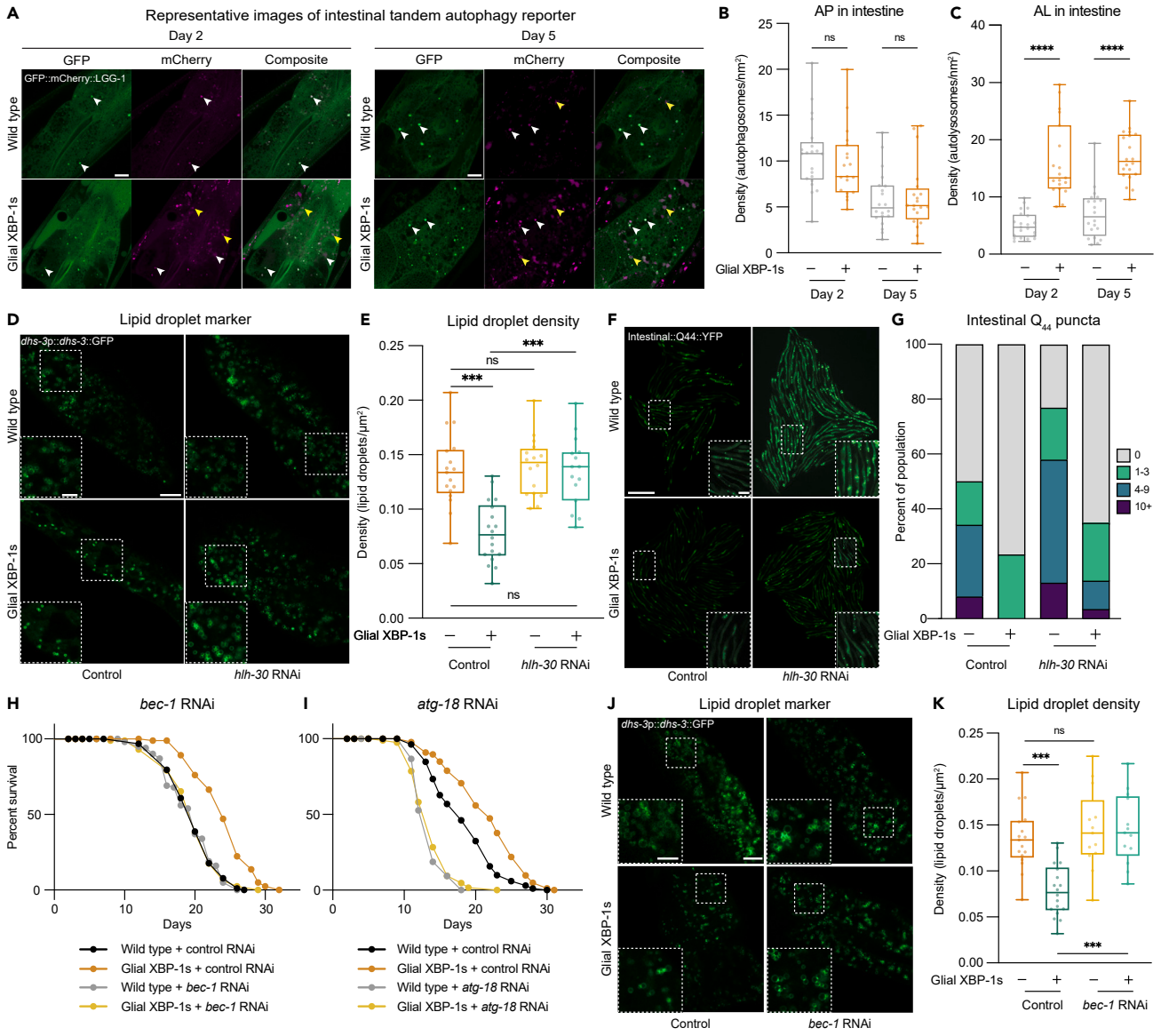

Figure 4. Glial XBP-1s cell non-autonomously activates peripheral autophagy, which is required for lifespan extension and reduced lipid levels

(A) Representative Airyscan micrographs from intestines of day 2 and day 5 wild-type and glial XBP-1s transgenic animals expressing the tandem autophagy reporter *mCherry::GFP::lgg-1* (green, GFP, magenta, mCherry). White arrowheads indicate autophagosomes, and yellow arrowheads indicate autolysosomes. Scale bar, 10 µm.

(B and C) Quantification of mCherry puncta co-localized with GFP (autophagosomes [AP]) (B) or containing mCherry alone (autolysosome [AL]) (C) in the intestine of wild-type and glial XBP-1s transgenic animals at day 2 and day 5 of adulthood. Data are from three independent experiments, each with ≥ 5 animals. Statistics by Kruskal-Wallis with Dunn's multiple comparison test, $p < 0.0001$ (****).

(D) Representative Airyscan micrographs of *dhs-3*p::*dhs-3*::GFP labeled lipid droplets from the intestine of day 2 wild-type and glial XBP-1s adult animals grown on HT115 *E. coli* expressing control or *hlh-30* RNAi. Scale bar, 10 µm. Scale bar of inset, 5 µm.

(E) Changes in lipid droplet density of wild-type and glial XBP-1s animals grown on control or *hlh-30* RNAi from (D). Boxplot shows median, whiskers are minimum to maximum values, each dot is representative of one animal. Statistics by Kruskal-Wallis with Dunn's multiple comparison test, $p < 0.001$ (***), $p > 0.05$ (ns). $N > 15$, and from three independent replicates.

(F) Representative fluorescent micrographs of age-dependent accumulation of transgenic polyQ$_{44}$-YFP aggregates in wild-type or glial XBP-1s animals grown on control or *hlh-30* RNAi. Scale bar, 1 mm. Scale bar of inset, 200 µm.

(G) Quantification of age-dependent polyQ$_{44}$ aggregates from (F), grouped into animals with 0 (gray), 1–3 (green), 4–9 (blue), or >10 (purple) aggregates. $N > 100$ per condition. Data are representative from three independent replicates. Statistics done by Chi-squared test for independence with adjusted residual and Bonferroni correction, statistics shown in Table S4.

Figure 4. *Continued*

(H and I) Survival of wild-type and glial XBP-1s animals on control, *bec-1* (D) or *atg-18* RNAi (E) at 20°C. Lifespan is representative of three independent replicates. See Table S1for lifespan statistics.

(J) Representative Airyscan micrographs of transgenic *dhs-3*p::*dhs-3*::GFP labeled lipid droplets from the intestine of day 2 wild-type and glial XBP-1s adults grown on control or *bec-1* RNAi. Scale bar, 10 μm. Scale bar of inset, 5 μm.

(K) Changes in lipid droplet density of wild-type and glial XBP-1s animals grown on control or *bec-1* RNAi from (J). Boxplot shows median, whiskers are minimum to maximum values. Statistics by Kruskal-Wallis with Dunn's multiple comparison test, $p < 0.001$ (***). $N > 15$ per condition from three independent replicates.

neurodegenerative disorders, such as Huntington's disease, and when expressed in *C. elegans* can model such protein-folding disorders and serve as a proxy for proteostasis capacity.[63,64] We examined the number of intestinal polyQ-YFP aggregates in adulthood and found that the reduction of aggregates in glial XBP-1s animals is dependent on *hlh-30* (Figures 4F, 4G, and S4D). These data indicate that the glial XBP-1s paradigm protects against intestinal polyQ aggregation through the activity of HLH-30.

Macroautophagy is required for lifespan extension and lipid droplet depletion in glial XBP-1s animals

The ability to activate autophagy declines with age and is increased in numerous conserved longevity paradigms.[60] We observed an increase in the expression of autophagy genes (Figure S4C) and increased autophagic capacity in glial XBP-1s animals (Figures 4A–4C). Therefore, we tested if autophagy genes are required for the lifespan extension of glial XBP-1s animals. Knockdown by RNAi of autophagy genes that are required for the induction of macroautophagy, *bec-1* (autophagosome membrane nucleation) and *atg-18* (phosphoinositide 3-phosphate binding), abrogated the lifespan extension of glial XBP-1s animals (Figures 4H and 4I). These data indicate that macroautophagy is required for lifespan extension in glial XBP-1s animals.

Lipid catabolism is driven through lipophagy, the autophagic degradation of lipid droplets, and lipolysis in lysosomes. We found an expansion of lysosomes, upregulation of HLH-30 lipid catabolism genes, and a dependence on *hlh-30* for lipid depletion in the intestines of glial XBP-1s animals. Therefore, we hypothesized that this depletion is caused by macroautophagy of lipid droplets. We found that knockdown of *bec-1* fully suppresses the lipid droplet depletion found in glial XBP-1s animals (Figures 4J and 4K).

Altered ER structures in glial XBP-1s animals are dependent on macroautophagy genes and co-localize with autophagosomes and autolysosomes

After seeing changes in autophagic activation concurrent with HLH-30 activation, we asked whether the changes in ER morphology detected in glial XBP-1s animals (Figures 1I and 1J) are dependent on autophagy.[43] ERphagy, the selective degradation of the ER by autophagy, plays a major role in maintaining ER homeostasis and is involved in the recovery from ER stress.[65] We found that the formation of the ER structures seen in glial XBP-1s animals is dependent on macroautophagy in the intestine. Knockdown of core components of the macroautophagy machinery, *atg-18*, *vps-34* (kinase that recruits machinery to form autophagosomes), *bec-1*, and *lgg-1* (involved in phagophore elongation and cargo recruitment) resolved the formation of the ER puncta detected in glial XBP-1s animals (Figures 5A and 5B).

Intriguingly, when determining the dependence on the ER puncta formation on neuropeptide, via *egl-3(ok979)* mutation or DCV release, via *unc-31(e928)* mutation, we found that knockout of these genes did not completely suppress the formation of the ER puncta in glial XBP-1s animals (Figures S4F and S4G). Glial XBP-1s animals with the *unc-31(e928)* mutation had a decrease in ER puncta density down to the levels of *unc-31(e928)* mutants alone, while the *egl-3(ok979)* mutation did not significantly suppress the formation of ER puncta. Interestingly, we observed that *egl-3(ok979)* and *unc-31(e928)* mutations were sufficient to induce ER puncta. Since the *egl-3(ok979)* and *unc-31(e928)* mutations have increased autophagy (Figure S4E), the increase in autophagy in both these mutants and in glial XBP-1s animals may be driving the formation of these ER structures.

We next investigated if these ER puncta colocalized with markers for lysosomes and autophagosomes. Staining for lysosomes using LysoTracker, a pH-dependent dye that accumulates in acidic lysosomes, in the mRuby:HDEL (ER) strains showed significant colocalization of lysosomes with mRuby:HDEL puncta in glial XBP-1s compared to wild-type animals (Figures 5C and 5E). Using a strain expressing GFP-tagged LGG-1, a protein that localizes to autophagosomal membranes, we found that glial XBP-1s animals have significant colocalization of mRuby:HDEL (ER) and LGG-1:GFP positive puncta (Figures 5D and 5F). We next asked if the circular ER structures we visualized using high-magnification TEM (Figure 1I) were dependent on autophagy activation. Strikingly, we found that knockdown of *bec-1* in glial XBP-1s resolved the formation of these structures (Figures 5G and S4H). Taken together, these results suggest that *xbp-1s* expression in CEPsh glia leads to cell non-autonomous restructured distal ER, which is dependent on macroautophagy components and colocalizes with autophagosomes and lysosomes, indicative of ERphagy activation.

DISCUSSION

In this work, we have found that CEPsh glial cells of *C. elegans* coordinate peripheral metabolism, autophagy activation, and ER remodeling when the UPR^{ER} is activated in these four cells. Ectopic expression of constitutively active *xbp-1s* in CEPsh glia leads to significant lipid depletion and ER remodeling in the intestine. We find that the transcription factor HLH-30 has significant nuclear localization in intestinal tissue and partly controls the expression of a third of genes upregulated in glial XBP-1s animals (Figure 6). Interestingly, mutations in genes required for DCV exocytosis (*unc-31*), suppressed this cell non-autonomous activation of HLH-30 in glial XBP-1s animals. *hlh-30* is required for the significant lifespan extension, reduction in lipid content, and increased intestinal proteostasis found in glial XBP-1s animals. We also find that

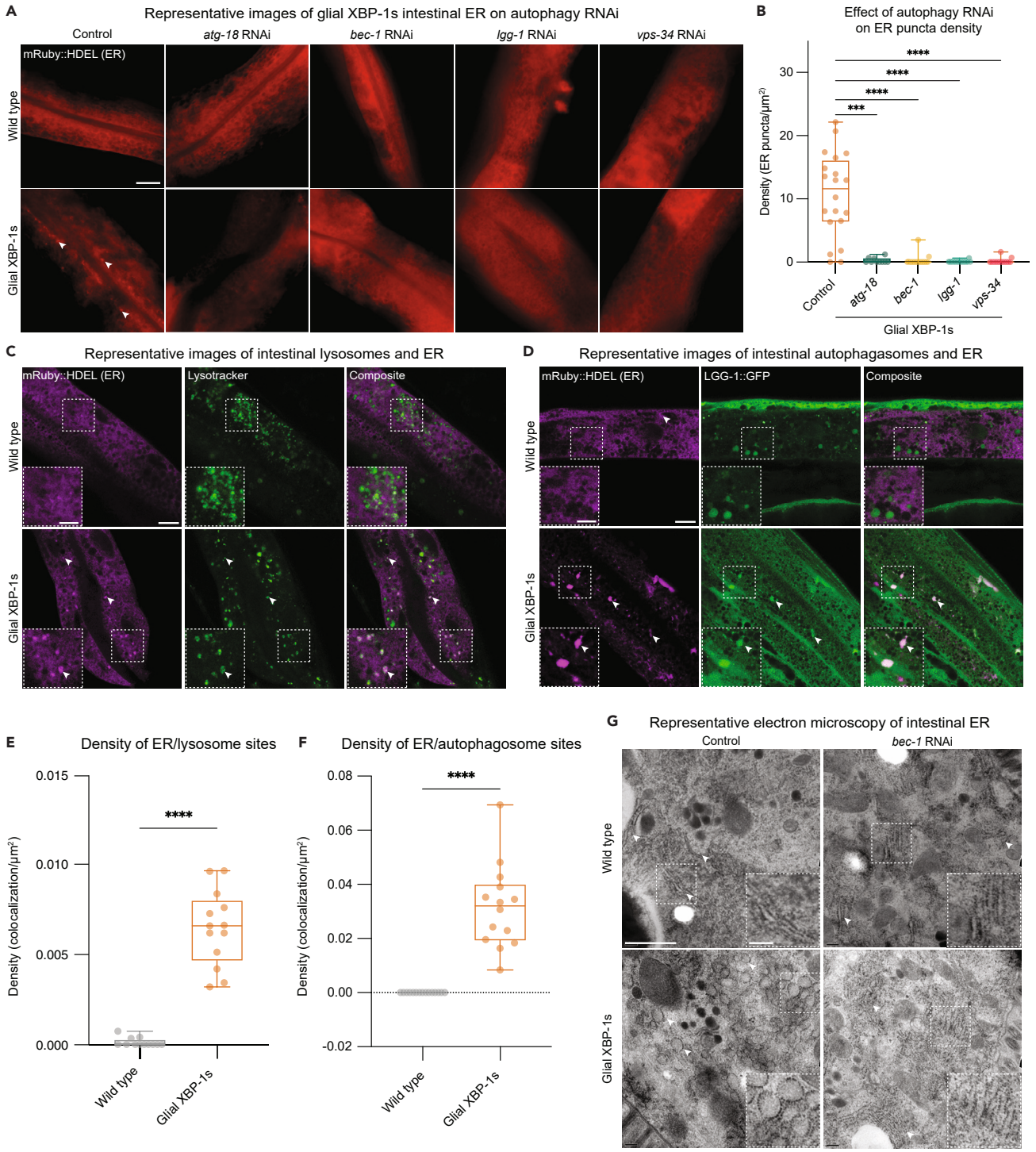

Figure 5. Macroautophagy is required for changes in intestinal ER morphology and lipid depletion in glial XBP-1s animals

(A) Representative Airyscan micrographs from intestine of day 2 wild-type and glial XBP-1s animals transgenic for the ER marker *vha-6p*::ERss:mRuby:HDEL, animals were grown on control or the corresponding RNAi. ER puncta is denoted by arrowheads.

(B) Quantification of ER puncta from (A). Density was determined by counting the number of ER puncta per area of intestine expressing *vha-6p*::ERss:mRuby:HDEL. N > 15 per condition from three independent replicates. Statistics by Kruskal-Wallis with Dunn's multiple comparison test, $p < 0.001$ (***), $p < 0.0001$ (****).

Figure 5. *Continued*

(C) Representative Airyscan micrographs from intestines of day 2 wild-type and glial XBP-1s animals transgenic for the ER marker *vha-6p*::ERss:mRuby:HDEL (pseudo-colored in magenta) and stained with Lysotracker Blue DND-22 (pseudo-colored in green). Arrowheads mark colocalization. Scale bar, 10 μm. Scale bar of inset, 5 μm.

(D) Representative Airyscan micrographs from intestine of day 2 wild-type and glial XBP-1s animals transgenic for the ER marker *vha-6p*::ERss:mRuby:HDEL (magenta) and autophagosome marker LGG-1:GFP (green). Arrowheads mark colocalization. Scale bar, 10 μm. Scale bar of inset, 5 μm.

(E) Quantification of density of ER puncta and lysotracker colocalization. Statistics by Mann-Whitney test, $p < 0.0001$ (****). $N > 15$ per condition from three independent replicates.

(F) Quantification of density of ER puncta and autophagosome colocalization. Statistics by Mann-Whitney test, $p < 0.0001$ (****). $N > 15$ per condition from three independent replicates.

(G) Electron micrographs of intestine from wild-type and glial XBP-1s animals at day 2 of adulthood grown on either empty vector control or *bec-1* RNAi. Imaging was replicated in triplicate for a total of 15–20 animals being imaged per condition. Arrowheads mark rough endoplasmic reticulum. Scale bar, 1μm. Scale bar of inset, 0.2 μm.

ectopic *xbp-1s* expression leads to cell non-autonomous activation of autophagy in the periphery and that autophagy regulators are required for lifespan extension and lipid depletion. Lastly, the ER morphological changes seen in glial XBP-1s animals are dependent on macroautophagy, colocalize with autophagosomes and lysosomes, and may be suggestive of ER-phagy occurring peripherally. Taken together, these data describe a novel role of communication from UPR^{ER} activation in glial cells to the periphery which regulates organismal metabolism and autophagy activation that cannot be achieved by cell autonomous UPR^{ER} activation.

This work has shown that glial cells have crucial roles in the regulation of organismal autophagy and lipid metabolism beyond the nervous system. Previous work has shown that pan-neuronal ectopic expression of XBP-1s in *C. elegans* regulates cell non-autonomous UPR activation in the gut to extend lifespan and increase stress resistance.[3] Communication between neurons and the intestine depends upon SCV release of neurotransmitters, improving lysosome activity, and lipid metabolism.[21–25] In contrast, glial cell non-autonomous activation of the UPR^{ER} and lifespan extension is dependent on neuropeptides released from DCVs (DCV).[2] Additionally, we find DCV-dependent activation of HLH-30 in glial XBP-1s animals, in contrast to neuronal XBP-1s animals that do not activate HLH-30 peripherally.[21] These data suggest that glial cells communicate with the periphery to coordinate the induction of lipid catabolism and lysosome activation through a mechanism independent and distinct from that of neurons, which is dependent on the neurotransmitters tyramine, acetylcholine, serotonin, and dopamine.[22,23] Further studies into the origin and nature of this glial signal, which in *C. elegans* may act as a primitive hormone signal, are of great interest. Discovery of the relevant glial signal would identify therapeutic interventions to potentially reverse age-onset proteome and autophagic decline seen in neurodegenerative and metabolic diseases.

The transcription factor TFEB/HLH-30 controls lysosomal biogenesis and autophagy by regulating the expression of genes in the coordinated lysosomal expression and regulation (CLEAR) network.[55] Interestingly, knockout of *Tfeb* in hepatocytes of mice leads to impaired lipid degradation pathways in these cells.[53] Conversely, overexpression of *Tfeb* in liver cells of mice fed a high-fat diet or in obese mice, caused by a homozygous mutation in the gene responsible for the production of leptin (*ob/ob*), a hormone responsible for regulating energy balance by inhibiting hunger, attenuates the development of obesity.[53] In *C. elegans*, HLH-30 couples nutrient availability to transcription of lysosomal lipases and autophagy, controlling fat storage and aging.[54] It was recently found that XBP1s regulates autophagy in murine liver cells through the activation of TFEB. Overexpression of *Xbp-1s* enhanced TFEB transcription and autophagy, while overexpression of *Tfeb* ameliorated the glucose intolerance seen in *Xbp1* liver knockout mice with diet-induced obesity.[66] Our findings implicate numerous genes being co-regulated by both XBP-1s and HLH-30 in these glial XBP-1s animals. Further investigation into the XBP-1s/HLH-30 axis and how these pathways converge in metabolic health and dysfunction is warranted.

The failure of the UPR^{ER} to function properly is a hallmark of numerous age-related neurodegenerative and metabolic disorders. In states of chronic overnutrition, the UPR^{ER} machinery can be overwhelmed, leading to persistent and unresolved ER stress. Mice that are heterozygous for a null XBP-1 allele develop glucose intolerance, severe insulin resistance, and diabetes.[67] Additionally, *ob/ob* mice have impaired UPR^{ER} signaling and decreased nuclear localization of XBP-1s in their livers.[68] Interestingly, mice with a conditional deletion of *Xbp-1* in neurons and glia are more susceptible to diet-induced obesity and become leptin-resistant.[69] Surprisingly, activation of XBP-1s in hypothalamic pro-opiomelanocortin (POMC) neurons of mice leads to cell non-autonomous induction of the UPR^{ER} in the liver, which protects the mice from diet-induced obesity and helps maintain metabolic homeostasis.[4] Cell non-autonomous activation of the UPR^{ER} from neurons to the periphery has also been seen in physiological settings, food perception alone in mice induces global metabolic changes involving systemic UPR^{ER} activation.[5] This cell non-autonomous signaling of the UPR^{ER} points to a conserved mechanism of global control of organismal metabolic homeostasis by neural UPR^{ER} activation. Interrogating the potential role of mammalian glial XBP-1s as a therapeutic target in these chronic metabolic disorders is therefore of great interest.

Because glia have critical roles in providing metabolic support for neurons, we speculate that they are well-positioned to integrate the metabolic state of the brain and mediate communication with peripheral tissues. It is hypothesized that glial cells first evolved as static support cells for neurons, but with increasing nervous system complexity their roles shifted to increase neural function capacity and to generate efficient energy metabolism in the nervous system.[70,71] There are numerous subpopulations of glial cell types that are positioned at major cruxes of metabolism, including astrocytes in the hypothalamus, tanycytes in contact with both the cerebral spinal fluid and the arcuate nucleus of the hypothalamus, and enteric glia in the gut-brain axis.[72–74] In humans, the brain is the primary consumer of glucose, using a fifth of total ATP stores, primarily from glucose in blood circulation, with glial cells playing a critical role in the transport of glucose.[75] In the CNS, glial cells uptake glucose and generate glycolysis-derived lactate which is transported into neurons where it is then metabolized to acetyl

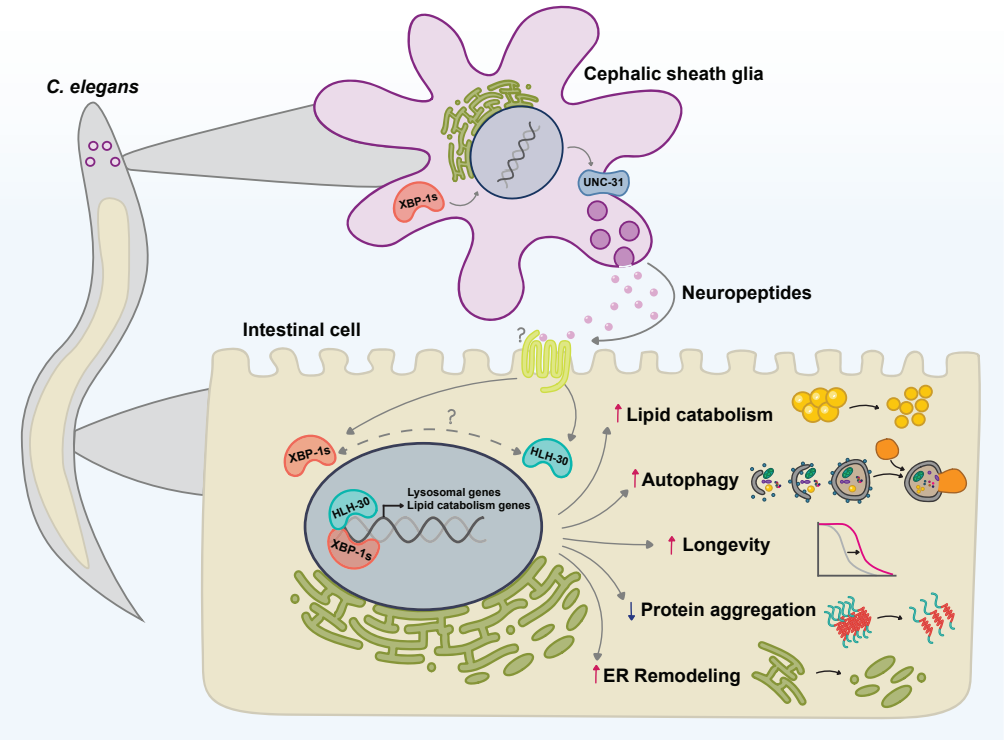

Figure 6. Schematic of glial XBP-1s effects on peripheral metabolism and autophagy

Expression of *xbp-1s* in the four CEPsh glia induces activation of the UPR^{ER} and the transcription factor HLH-30/TFEB in the periphery, reliant on exocytosis of dense core vesicles (*unc-31*). HLH-30 regulates the transcription of lipid catabolism and lysosomal biogenesis genes in glial XBP-1s animals. HLH-30 is required for increased lipid catabolism, activated autophagy, decreased intestinal protein aggregation, lifespan extension, and ER remodeling in glial XBP-1s animals. Autophagy induction is also required for longevity, lipid catabolism, and ER remodeling phenotypes in the glial XBP-1s paradigm. These data suggest that glia provide cell non-autonomous control over peripheral autophagy and metabolic adaptation during stress.

coenzyme A, a key energy input into the tricarboxylic acid cycle.[76] Additionally, two separate studies have shown that insulin signaling in hypothalamic astrocytes and tanycytes is required for brain glucose sensing and systemic glucose metabolism.[72,73] Further identification of the processes that are specific to glial XBP-1s regulation of neuronal and systemic metabolic homeostasis is warranted.

Here, we show that glia play a critical role in coordinating peripheral metabolic homeostasis and autophagy activation via XBP-1s activation and cell non-autonomous activation of HLH-30. Activation of these processes relies solely on activation of *xbp-1s* in CEPsh glia. Neither HLH-30 overexpression in glial cells nor cell autonomous induction of the UPR^{ER} can turn on these processes in the periphery. We believe that glial communication of ER stress is an advantageous organismal adaptation by which detection of ER stress can be sensed and systemically transmitted to promote longevity, stress resistance, and metabolic health. Our work furthers the argument of the UPR^{ER} being a major sensor and coordinator of organismal homeostasis and highlights the important roles of glial cells in coordinating systemic metabolism and proteostasis. The evolution of this process in metazoa ensures the communication of stress and metabolism across cell and organ systems to promote the health of the entire organism.

STAR★METHODS

Detailed methods are provided in the online version of this paper and include the following:

- KEY RESOURCES TABLE
- RESOURCE AVAILABILITY
  - Lead contact
  - Materials availability
  - Data and code availability
- EXPERIMENTAL MODEL AND SUBJECT DETAILS
  - *C. elegans* strains and details
- METHOD DETAILS
  - Lifespan analysis

SUPPLEMENTAL INFORMATION

Supplemental information can be found online at https://doi.org/10.1016/j.isci.2024.109354.

ACKNOWLEDGMENTS

We thank the Caenorhabditis Genetics Center (CGC) (P40 OD010440) for several strains used in this study and the Dillin lab for comments and discussion throughout the project. M.G.M was supported by the NIH (F31 AG060660). A.E.F. was supported by the NIH (F32 AG051355). A.D. is supported by the Thomas and Stacey Siebel Foundation, the Howard Hughes Medical Institute, and NIH grants R37 AG024365, R01 ES021667, R01 AG055891, and R01 AG059566.

AUTHOR CONTRIBUTIONS

M.G.M. conceived the project. M.G.M., S.M., A.S., J.D., A.E.F., M.V., C.M., A.F., and M.S. performed experiments. M.G.M., S.M., A.E.F., A.S., M.V., and A.F. analyzed data. A.D. supervised the project. M.G.M. wrote the manuscript with input from all authors.

DECLARATION OF INTERESTS

The authors declare that they have no competing interests.

Received: May 16, 2022
Revised: November 1, 2023
Accepted: February 23, 2024
Published: February 28, 2024

REFERENCES

1. García-Cáceres, C., Balland, E., Prevot, V., Luquet, S., Woods, S.C., Koch, M., Horvath, T.L., Yi, C.X., Chowen, J.A., Verkhratsky, A., et al. (2019). Role of astrocytes, microglia, and tanycytes in brain control of systemic metabolism. Nat. Neurosci. *22*, 7–14. https://doi.org/10.1038/s41593-018-0286-y.
2. Frakes, A.E., Metcalf, M.G., Tronnes, S.U., Bar-Ziv, R., Durieux, J., Gildea, H.K., Kandahari, N., Monshietehadi, S., and Dillin, A. (2020). Four glial cells regulate ER stress resistance and longevity via neuropeptide signaling in C. elegans. Science *367*, 436–440. https://doi.org/10.1126/science.aaz6896.
3. Taylor, R.C., and Dillin, A. (2013). XBP-1 is a cell-nonautonomous regulator of stress resistance and longevity. Cell *153*, 1435–1447. https://doi.org/10.1016/j.cell.2013.05.042.
4. Williams, K.W., Liu, T., Kong, X., Fukuda, M., Deng, Y., Berglund, E.D., Deng, Z., Gao, Y., Liu, T., Sohn, J.W., et al. (2014). Xbp1s in Pomc neurons connects ER stress with energy balance and glucose homeostasis. Cell Metabol. *20*, 471–482. https://doi.org/10.1016/j.cmet.2014.06.002.
5. Brandt, C., Nolte, H., Henschke, S., Engström Ruud, L., Awazawa, M., Morgan, D.A., Gabel, P., Sprenger, H.G., Hess, M.E., Günther, S., et al. (2018). Food Perception Primes Hepatic ER Homeostasis via Melanocortin-Dependent Control of mTOR Activation. Cell *175*, 1321–1335.e20. https://doi.org/10.1016/j.cell.2018.10.015.
6. Durieux, J., Wolff, S., and Dillin, A. (2011). The cell-non-autonomous nature of electron transport chain-mediated longevity. Cell *144*, 79–91. https://doi.org/10.1016/j.cell.2010.12.016.
7. Camandola, S., and Mattson, M.P. (2017). Brain metabolism in health, aging, and neurodegeneration. EMBO J. *36*, 1474–1492. https://doi.org/10.15252/embj.201695810.
8. Mayorga-Weber, G., Rivera, F.J., and Castro, M.A. (2022). Neuron-glia (mis)interactions in brain energy metabolism during aging. J. Neurosci. Res. *100*, 835–854. https://doi.org/10.1002/jnr.25015.
9. Hipp, M.S., Kasturi, P., and Hartl, F.U. (2019). The proteostasis network and its decline in ageing. Nat. Rev. Mol. Cell Biol. *20*, 421–435. https://doi.org/10.1038/s41580-019-0101-y.
10. Oakes, S.A., and Papa, F.R. (2015). The role of endoplasmic reticulum stress in human pathology. Annu. Rev. Pathol. *10*, 173–194. https://doi.org/10.1146/annurev-pathol-012513-104649.
11. Metcalf, M.G., Higuchi-Sanabria, R., Garcia, G., Tsui, C.K., and Dillin, A. (2020). Beyond the cell factory: Homeostatic regulation of and by the UPR(ER). Sci. Adv. *6*, eabb9614. https://doi.org/10.1126/sciadv.abb9614.
12. Sidrauski, C., and Walter, P. (1997). The transmembrane kinase Ire1p is a site-specific endonuclease that initiates mRNA splicing in the unfolded protein response. Cell *90*, 1031–1039. https://doi.org/10.1016/s0092-8674(00)80369-4.
13. Calfon, M., Zeng, H., Urano, F., Till, J.H., Hubbard, S.R., Harding, H.P., Clark, S.G., and Ron, D. (2002). IRE1 couples endoplasmic reticulum load to secretory capacity by

processing the XBP-1 mRNA. Nature *415*, 92–96. https://doi.org/10.1038/415092a.
14. Fu, S., Watkins, S.M., and Hotamisligil, G.S. (2012). The role of endoplasmic reticulum in hepatic lipid homeostasis and stress signaling. Cell Metabol. *15*, 623–634. https://doi.org/10.1016/j.cmet.2012.03.007.
15. Cox, J.S., Chapman, R.E., and Walter, P. (1997). The unfolded protein response coordinates the production of endoplasmic reticulum protein and endoplasmic reticulum membrane. Mol. Biol. Cell *8*, 1805–1814. https://doi.org/10.1091/mbc.8.9.1805.
16. Kono, N., Amin-Wetzel, N., and Ron, D. (2017). Generic membrane-spanning features endow IRE1alpha with responsiveness to membrane aberrancy. Mol. Biol. Cell *28*, 2318–2332. https://doi.org/10.1091/mbc.E17-03-0144.
17. Promlek, T., Ishiwata-Kimata, Y., Shido, M., Sakuramoto, M., Kohno, K., and Kimata, Y. (2011). Membrane aberrancy and unfolded proteins activate the endoplasmic reticulum stress sensor Ire1 in different ways. Mol. Biol. Cell *22*, 3520–3532. https://doi.org/10.1091/mbc.E11-04-0295.
18. Yamamoto, K., Sato, T., Matsui, T., Sato, M., Okada, T., Yoshida, H., Harada, A., and Mori, K. (2007). Transcriptional induction of mammalian ER quality control proteins is mediated by single or combined action of ATF6alpha and XBP1. Dev. Cell *13*, 365–376. https://doi.org/10.1016/j.devcel.2007.07.018.
19. Adamson, B., Norman, T.M., Jost, M., Cho, M.Y., Nuñez, J.K., Chen, Y., Villalta, J.E., Gilbert, L.A., Horlbeck, M.A., Hein, M.Y., et al. (2016). A Multiplexed Single-Cell CRISPR Screening Platform Enables Systematic Dissection of the Unfolded Protein Response. Cell *167*, 1867–1882.e21. https://doi.org/10.1016/j.cell.2016.11.048.
20. Piperi, C., Adamopoulos, C., and Papavassiliou, A.G. (2016). XBP1: A Pivotal Transcriptional Regulator of Glucose and Lipid Metabolism. Trends Endocrinol. Metabol. *27*, 119–122. https://doi.org/10.1016/j.tem.2016.01.001.
21. Imanikia, S., Özbey, N.P., Krueger, C., Casanueva, M.O., and Taylor, R.C. (2019). Neuronal XBP-1 Activates Intestinal Lysosomes to Improve Proteostasis in C. elegans. Curr. Biol. *29*, 2322–2338.e7. https://doi.org/10.1016/j.cub.2019.06.031.
22. Özbey, N.P., Imanikia, S., Krueger, C., Hardege, I., Morud, J., Sheng, M., Schafer, W.R., Casanueva, M.O., and Taylor, R.C. (2020). Tyramine Acts Downstream of Neuronal XBP-1s to Coordinate Inter-tissue UPR(ER) Activation and Behavior in C. elegans. Dev. Cell *55*, 754–770.e6. https://doi.org/10.1016/j.devcel.2020.10.024.
23. Higuchi-Sanabria, R., Durieux, J., Kelet, N., Homentcovschi, S., de Los Rios Rogers, M., Monshietehadi, S., Garcia, G., Dallarda, S., Daniele, J.R., Ramachandran, V., et al. (2020). Divergent Nodes of Non-autonomous UPR(ER) Signaling through Serotonergic and Dopaminergic Neurons. Cell Rep. *33*, 108489. https://doi.org/10.1016/j.celrep.2020.108489.
24. Imanikia, S., Sheng, M., Castro, C., Griffin, J.L., and Taylor, R.C. (2019). XBP-1 Remodels Lipid Metabolism to Extend Longevity. Cell Rep. *28*, 581–589.e4. https://doi.org/10.1016/j.celrep.2019.06.057.
25. Daniele, J.R., Higuchi-Sanabria, R., Durieux, J., Monshietehadi, S., Ramachandran, V., Tronnes, S.U., Kelet, N., Sanchez, M., Metcalf, M.G., Garcia, G., et al. (2020). UPR(ER) promotes lipophagy independent of chaperones to extend life span. Sci. Adv. *6*, eaaz1441. https://doi.org/10.1126/sciadv.aaz1441.
26. Singhvi, A., and Shaham, S. (2019). Glia-Neuron Interactions in Caenorhabditis elegans. Annu. Rev. Neurosci. *42*, 149–168. https://doi.org/10.1146/annurev-neuro-070918-050314.
27. Katz, M., Corson, F., Iwanir, S., Biron, D., and Shaham, S. (2018). Glia Modulate a Neuronal Circuit for Locomotion Suppression during Sleep in C. elegans. Cell Rep. *22*, 2575–2583. https://doi.org/10.1016/j.celrep.2018.02.036.
28. Katz, M., Corson, F., Keil, W., Singhal, A., Bae, A., Lu, Y., Liang, Y., and Shaham, S. (2019). Glutamate spillover in C. elegans triggers repetitive behavior through presynaptic activation of MGL-2/mGluR5. Nat. Commun. *10*, 1882. https://doi.org/10.1038/s41467-019-09581-4.
29. Rapti, G., Li, C., Shan, A., Lu, Y., and Shaham, S. (2017). Glia initiate brain assembly through noncanonical Chimaerin-Furin axon guidance in C. elegans. Nat. Neurosci. *20*, 1350–1360. https://doi.org/10.1038/nn.4630.
30. Lago-Baldaia, I., Fernandes, V.M., and Ackerman, S.D. (2020). More Than Mortar: Glia as Architects of Nervous System Development and Disease. Front. Cell Dev. Biol. *8*, 611269. https://doi.org/10.3389/fcell.2020.611269.
31. Lapierre, L.R., De Magalhaes Filho, C.D., McQuary, P.R., Chu, C.C., Visvikis, O., Chang, J.T., Gelino, S., Ong, B., Davis, A.E., Irazoqui, J.E., et al. (2013). The TFEB orthologue HLH-30 regulates autophagy and modulates longevity in Caenorhabditis elegans. Nat. Commun. *4*, 2267. https://doi.org/10.1038/ncomms3267.
32. López-Otín, C., Galluzzi, L., Freije, J.M.P., Madeo, F., and Kroemer, G. (2016). Metabolic Control of Longevity. Cell *166*, 802–821. https://doi.org/10.1016/j.cell.2016.07.031.
33. Singh, P.P., Demmitt, B.A., Nath, R.D., and Brunet, A. (2019). The Genetics of Aging: A Vertebrate Perspective. Cell *177*, 200–220. https://doi.org/10.1016/j.cell.2019.02.038.
34. Templeman, N.M., and Murphy, C.T. (2018). Regulation of reproduction and longevity by nutrient-sensing pathways. J. Cell Biol. *217*, 93–106. https://doi.org/10.1083/jcb.201707168.
35. Klapper, M., Ehmke, M., Palgunow, D., Böhme, M., Matthäus, C., Bergner, G., Dietzek, B., Popp, J., and Döring, F. (2011). Fluorescence-based fixative and vital staining of lipid droplets in Caenorhabditis elegans reveal fat stores using microscopy and flow cytometry approaches. J. Lipid Res. *52*, 1281–1293. https://doi.org/10.1194/jlr.D011940.
36. Mak, H.Y. (2012). Lipid droplets as fat storage organelles in Caenorhabditis elegans: Thematic Review Series: Lipid Droplet Synthesis and Metabolism: from Yeast to Man. J. Lipid Res. *53*, 28–33. https://doi.org/10.1194/jlr.R021006.
37. Na, H., Zhang, P., Chen, Y., Zhu, X., Liu, Y., Liu, Y., Xie, K., Xu, N., Yang, F., Yu, Y., et al. (2015). Identification of lipid droplet structure-like/resident proteins in Caenorhabditis elegans. Biochim. Biophys. Acta *1853*, 2481–2491. https://doi.org/10.1016/j.bbamcr.2015.05.020.
38. Thelen, A.M., and Zoncu, R. (2017). Emerging Roles for the Lysosome in Lipid Metabolism. Trends Cell Biol. *27*, 833–850. https://doi.org/10.1016/j.tcb.2017.07.006.
39. Lawrence, R.E., and Zoncu, R. (2019). The lysosome as a cellular centre for signalling, metabolism and quality control. Nat. Cell Biol. *21*, 133–142. https://doi.org/10.1038/s41556-018-0244-7.
40. Singh, R., Kaushik, S., Wang, Y., Xiang, Y., Novak, I., Komatsu, M., Tanaka, K., Cuervo, A.M., and Czaja, M.J. (2009). Autophagy regulates lipid metabolism. Nature *458*, 1131–1135. https://doi.org/10.1038/nature07976.
41. Song, B.M., and Avery, L. (2013). The pharynx of the nematode C. elegans: A model system for the study of motor control. Worm *2*, e21833. https://doi.org/10.4161/worm.21833.
42. van Meer, G., Voelker, D.R., and Feigenson, G.W. (2008). Membrane lipids: where they are and how they behave. Nat. Rev. Mol. Cell Biol. *9*, 112–124. https://doi.org/10.1038/nrm2330.
43. Bernales, S., McDonald, K.L., and Walter, P. (2006). Autophagy counterbalances endoplasmic reticulum expansion during the unfolded protein response. PLoS Biol. *4*, e423. https://doi.org/10.1371/journal.pbio.0040423.
44. Schuck, S., Prinz, W.A., Thorn, K.S., Voss, C., and Walter, P. (2009). Membrane expansion alleviates endoplasmic reticulum stress independently of the unfolded protein response. J. Cell Biol. *187*, 525–536. https://doi.org/10.1083/jcb.200907074.
45. Sriburi, R., Jackowski, S., Mori, K., and Brewer, J.W. (2004). XBP1: a link between the unfolded protein response, lipid biosynthesis, and biogenesis of the endoplasmic reticulum. J. Cell Biol. *167*, 35–41. https://doi.org/10.1083/jcb.200406136.
46. Sriburi, R., Bommiasamy, H., Buldak, G.L., Robbins, G.R., Frank, M., Jackowski, S., and Brewer, J.W. (2007). Coordinate regulation of phospholipid biosynthesis and secretory pathway gene expression in XBP-1(S)-induced endoplasmic reticulum biogenesis. J. Biol. Chem. *282*, 7024–7034. https://doi.org/10.1074/jbc.M609490200.
47. Grant, B., and Hirsh, D. (1999). Receptor-mediated endocytosis in the Caenorhabditis elegans oocyte. Mol. Biol. Cell *10*, 4311–4326. https://doi.org/10.1091/mbc.10.12.4311.
48. Panowski, S.H., Wolff, S., Aguilaniu, H., Durieux, J., and Dillin, A. (2007). PHA-4/Foxa mediates diet-restriction-induced longevity of C. elegans. Nature *447*, 550–555. https://doi.org/10.1038/nature05837.
49. Ogg, S., Paradis, S., Gottlieb, S., Patterson, G.I., Lee, L., Tissenbaum, H.A., and Ruvkun, G. (1997). The Fork head transcription factor DAF-16 transduces insulin-like metabolic and longevity signals in C. elegans. Nature *389*, 994–999. https://doi.org/10.1038/40194.
50. Lin, K., Dorman, J.B., Rodan, A., and Kenyon, C. (1997). daf-16: An HNF-3/forkhead family member that can function to double the life-span of Caenorhabditis elegans. Science *278*, 1319–1322. https://doi.org/10.1126/science.278.5341.1319.
51. Apfeld, J., O'Connor, G., McDonagh, T., DiStefano, P.S., and Curtis, R. (2004). The AMP-activated protein kinase AAK-2 links energy levels and insulin-like signals to lifespan in C. elegans. Genes Dev. *18*, 3004–3009. https://doi.org/10.1101/gad.1255404.
52. Greer, E.L., Dowlatshahi, D., Banko, M.R., Villen, J., Hoang, K., Blanchard, D., Gygi, S.P., and Brunet, A. (2007). An AMPK-FOXO pathway mediates longevity induced by a

novel method of dietary restriction in C. elegans. Curr. Biol. *17*, 1646–1656. https://doi.org/10.1016/j.cub.2007.08.047.

53. Settembre, C., De Cegli, R., Mansueto, G., Saha, P.K., Vetrini, F., Visvikis, O., Huynh, T., Carissimo, A., Palmer, D., Klisch, T.J., et al. (2013). TFEB controls cellular lipid metabolism through a starvation-induced autoregulatory loop. Nat. Cell Biol. *15*, 647–658. https://doi.org/10.1038/ncb2718.
54. O'Rourke, E.J., and Ruvkun, G. (2013). MXL-3 and HLH-30 transcriptionally link lipolysis and autophagy to nutrient availability. Nat. Cell Biol. *15*, 668–676. https://doi.org/10.1038/ncb2741.
55. Settembre, C., Di Malta, C., Polito, V.A., Garcia Arencibia, M., Vetrini, F., Erdin, S., Erdin, S.U., Huynh, T., Medina, D., Colella, P., et al. (2011). TFEB links autophagy to lysosomal biogenesis. Science *332*, 1429–1433. https://doi.org/10.1126/science.1204592.
56. Lin, X.X., Sen, I., Janssens, G.E., Zhou, X., Fonslow, B.R., Edgar, D., Stroustrup, N., Swoboda, P., Yates, J.R., 3rd, Ruvkun, G., and Riedel, C.G. (2018). DAF-16/FOXO and HLH-30/TFEB function as combinatorial transcription factors to promote stress resistance and longevity. Nat. Commun. *9*, 4400. https://doi.org/10.1038/s41467-018-06624-0.
57. Oki, S., Ohta, T., Shioi, G., Hatanaka, H., Ogasawara, O., Okuda, Y., Kawaji, H., Nakaki, R., Sese, J., and Meno, C. (2018). ChIP-Atlas: a data-mining suite powered by full integration of public ChIP-seq data. EMBO Rep. *19*, e46255. https://doi.org/10.15252/embr.201846255.
58. Grove, C.A., De Masi, F., Barrasa, M.I., Newburger, D.E., Alkema, M.J., Bulyk, M.L., and Walhout, A.J.M. (2009). A multiparameter network reveals extensive divergence between C. elegans bHLH transcription factors. Cell *138*, 314–327. https://doi.org/10.1016/j.cell.2009.04.058.
59. Visvikis, O., Ihuegbu, N., Labed, S.A., Luhachack, L.G., Alves, A.M.F., Wollenberg, A.C., Stuart, L.M., Stormo, G.D., and Irazoqui, J.E. (2014). Innate host defense requires TFEB-mediated transcription of cytoprotective and antimicrobial genes. Immunity *40*, 896–909. https://doi.org/10.1016/j.immuni.2014.05.002.
60. Chang, J.T., Kumsta, C., Hellman, A.B., Adams, L.M., and Hansen, M. (2017). Spatiotemporal regulation of autophagy during Caenorhabditis elegans aging. Elife *6*, e18459. https://doi.org/10.7554/eLife.18459.
61. Ailion, M., Inoue, T., Weaver, C.I., Holdcraft, R.W., and Thomas, J.H. (1999). Neurosecretory control of aging in Caenorhabditis elegans. USA *96*, 7394–7397. https://doi.org/10.1073/pnas.96.13.7394.
62. Hansen, M., Chandra, A., Mitic, L.L., Onken, B., Driscoll, M., and Kenyon, C. (2008). A role for autophagy in the extension of lifespan by dietary restriction in C. elegans. PLoS Genet. *4*, e24. https://doi.org/10.1371/journal.pgen.0040024.
63. Morley, J.F., Brignull, H.R., Weyers, J.J., and Morimoto, R.I. (2002). The threshold for polyglutamine-expansion protein aggregation and cellular toxicity is dynamic and influenced by aging in Caenorhabditis elegans. Proc. Natl. Acad. Sci. USA *99*, 10417–10422. https://doi.org/10.1073/pnas.152161099.
64. Lieberman, A.P., Shakkottai, V.G., and Albin, R.L. (2019). Polyglutamine Repeats in Neurodegenerative Diseases. Annu. Rev. Pathol. *14*, 1–27. https://doi.org/10.1146/annurev-pathmechdis-012418-012857.
65. Hübner, C.A., and Dikic, I. (2020). ER-phagy and human diseases. Cell Death Differ. *27*, 833–842. https://doi.org/10.1038/s41418-019-0444-0.
66. Zhang, Z., Qian, Q., Li, M., Shao, F., Ding, W.X., Lira, V.A., Chen, S.X., Sebag, S.C., Hotamisligil, G.S., Cao, H., and Yang, L. (2021). The unfolded protein response regulates hepatic autophagy by sXBP1-mediated activation of TFEB. Autophagy *17*, 1841–1855. https://doi.org/10.1080/15548627.2020.1788889.
67. Ozcan, U., Cao, Q., Yilmaz, E., Lee, A.H., Iwakoshi, N.N., Ozdelen, E., Tuncman, G., Görgün, C., Glimcher, L.H., and Hotamisligil, G.S. (2004). Endoplasmic reticulum stress links obesity, insulin action, and type 2 diabetes. Science *306*, 457–461. https://doi.org/10.1126/science.1103160.
68. Park, S.W., Herrema, H., Salazar, M., Cakir, I., Cabi, S., Basibuyuk Sahin, F., Chiu, Y.H., Cantley, L.C., and Ozcan, U. (2014). BRD7 regulates XBP1s' activity and glucose homeostasis through its interaction with the regulatory subunits of PI3K. Cell Metabol. *20*, 73–84. https://doi.org/10.1016/j.cmet.2014.04.006.
69. Ozcan, L., Ergin, A.S., Lu, A., Chung, J., Sarkar, S., Nie, D., Myers, M.G., Jr., and Ozcan, U. (2009). Endoplasmic reticulum stress plays a central role in development of leptin resistance. Cell Metabol. *9*, 35–51. https://doi.org/10.1016/j.cmet.2008.12.004.
70. Rey, S., Zalc, B., and Klämbt, C. (2021). Evolution of glial wrapping: A new hypothesis. Dev. Neurobiol. *81*, 453–463. https://doi.org/10.1002/dneu.22739.
71. Hartline, D.K. (2011). The evolutionary origins of glia. Glia *59*, 1215–1236. https://doi.org/10.1002/glia.21149.
72. García-Cáceres, C., Quarta, C., Varela, L., Gao, Y., Gruber, T., Legutko, B., Jastroch, M., Johansson, P., Ninkovic, J., Yi, C.X., et al. (2016). Astrocytic Insulin Signaling Couples Brain Glucose Uptake with Nutrient Availability. Cell *166*, 867–880. https://doi.org/10.1016/j.cell.2016.07.028.
73. Porniece Kumar, M., Cremer, A.L., Klemm, P., Steuernagel, L., Sundaram, S., Jais, A., Hausen, A.C., Tao, J., Secher, A., Pedersen, T.Å., et al. (2021). Insulin signalling in tanycytes gates hypothalamic insulin uptake and regulation of AgRP neuron activity. Nat. Metab. *3*, 1662–1679. https://doi.org/10.1038/s42255-021-00499-0.
74. Seguella, L., and Gulbransen, B.D. (2021). Enteric glial biology, intercellular signalling and roles in gastrointestinal disease. Nat. Rev. Gastroenterol. Hepatol. *18*, 571–587. https://doi.org/10.1038/s41575-021-00423-7.
75. Erbsloh, F., Bernsmeier, A., and Hillesheim, H. (1958). [The glucose consumption of the brain & its dependence on the liver]. Arch. Psychiatr. Nervenkr. Z. Gesamte Neurol. Psychiatr. *196*, 611–626. https://doi.org/10.1007/BF00344388.
76. Liu, L., MacKenzie, K.R., Putluri, N., Maletić-Savatić, M., and Bellen, H.J. (2017). The Glia-Neuron Lactate Shuttle and Elevated ROS Promote Lipid Synthesis in Neurons and Lipid Droplet Accumulation in Glia via APOE/D. Cell Metabol. *26*, 719–737.e6. https://doi.org/10.1016/j.cmet.2017.08.024.
77. Afgan, E., Baker, D., van den Beek, M., Blankenberg, D., Bouvier, D., Čech, M., Chilton, J., Clements, D., Coraor, N., Eberhard, C., et al. (2016). The Galaxy platform for accessible, reproducible and collaborative biomedical analyses: 2016 update. Nucleic Acids Res. *44*, W3–W10. https://doi.org/10.1093/nar/gkw343.
78. Sanvictores, T., and Davis, D.D. (2022). Histology, Rough Endoplasmic Reticulum. In StatPearls.

STAR★METHODS

KEY RESOURCES TABLE

REAGENT or RESOURCE	SOURCE	IDENTIFIER
Bacterial and virus strains		
OP50	CGC	N/A
HT115	CGC	N/A
DH5α	Invitrogen	N/A
Chemicals, peptides, and recombinant proteins		
Agarose, low melting	Sigma-Aldrich	A9414-10G
Bacto Peptone	Fisher Scientific	DF0118072
BD Difco granulated agar	VWR	90000–782
BODIPY 493/503	Thermo Fisher	D3922
Calcium Chloride dihydrate	VWR	97061–904
Chloroform	Sigma-Aldrich	34854
Cholesterol	Sigma-Aldrich	57-88-5
Formaldehyde Aqueous Solution (4%)	Electron Microscopy Sciences	157–4
IPTG dioxane free	Denville Scientific	CI8280-4
Isopropanol	Fisher Scientific	AC327272500
LB Broth Miller	Fisher Scientific	BP1426500
LysoTracker Blue DND-22	Thermo Fisher	L7525
Magnesium Sulfate heptahydrate	VWR	EM-MX0070-3
Potassium Hydroxide	Fisher Scientific	P250-500
Potassium Phosphate dibasic	VWR	EM-PX1570-2
Potassium Phosphate monobasic	VWR	EM-PX1565-5
Sodium Azide	Sigma-Aldrich	71289-50G
Sodium Chloride	EMD Millipore	SX0420-5
Sodium Phosphate dibasic	VWR	71003–472
SYBR-green PCR Master Mix	Thermo Fisher	4309155
Tetracycline Hydrochloride	Sigma-Aldrich	T7660-5G
Trizol	Fisher Scientific	15596018
Tunicamycin	Millipore	654380
Critical commercial assays		
QIAquick Gel Extraction Kit	Qiagen	28706
NEBNext Ultra II RNA Library Prep Kit for Illumina	New England Biolabs	E7775
QIAquick PCR Purification Kit	Qiagen	28106
QIAGEN RNeasy Mini Kit	Qiagen	74106
QIAprep Spin Miniprep Kit	Qiagen	27106
QuantiTect Reverse Transcriptase Kit	Qiagen	205311
Deposited data		
C. elegans RNaseq	Mendeley	https://data.mendeley.com/datasets/yztws2dh4h/1
Experimental models: Organisms/strains		
C. elegans: N2 (Bristol)	CGC	N2

(*Continued on next page*)

Continued

REAGENT or RESOURCE	SOURCE	IDENTIFIER
C. elegans: AGD1723: uthIs439[hlh-17p:xbp-1s, myo-2p:tdTomato]	Frakes et al. 2020[2]	AGD1723
C. elegans: AGD1724: uthIs440[hlh-17p:xbp-1s, myo-2p:tdTomato]	Frakes et al. 2020[2]	AGD1724
C. elegans: LIU1: ldrIs1[dhs-3p:dhs-3:GFP + unc-76(+)]	CGC	LIU1
C. elegans: AGD2110: uthIs439[hlh-17p:xbp-1s, myo-2p:tdTomato]; ldrIs1[dhs-3p:dhs-3:GFP + unc-76(+)]	This study	AGD2110
C. elegans: RT258: unc-119(ed3)III; pwIs50[lmp-1:GFP+Cbr-unc-119(+)]	CGC	RT258
C. elegans: AGD2976: uthIs439[hlh-17p:xbp-1s, myo-2p:tdTomato]; unc-119(ed3)III; pwIs50[lmp-1:GFP+Cbr-unc-119(+)]	This study	AGD2976
C. elegans: AGD2192: unc-119(ed3) III; uthSi60[vha-6p:ERss:mRuby:HDEL:unc-54 3′UTR cb-unc-119(+)] IV	Daniele et al. 2020[25]	AGD2192
C. elegans: AGD2196: uthIs440[hlh-17p:xbp-1s, myo-2p:tdTomato]; unc-119(ed3) III; uthSi60[vha-6p:ERss:mRuby:HDEL: unc-54 3′UTR cb-unc-119(+)] IV	This study	AGD2196
C. elegans: AGD2287: uthIs440[hlh-17p:xbp-1s, myo-2p:tdTomato]; unc-119(ed3) III; uthSi60[vha-6p:ERss:mRuby:HDEL: unc-54 3′UTR cb-unc-119(+)] IV; egl-3(ok979)V	This study	AGD2287
C. elegans: AGD2318: uthIs440[hlh-17p:xbp-1s, myo-2p:tdTomato]; unc-119(ed3) III; uthSi60[vha-6p:ERss:mRuby:HDEL: unc-54 3′UTR cb-unc-119(+)] IV; unc-31(e928)IV	This study	AGD2318
C. elegans: MAH240: sqIs17[hlh-30p:hlh-30:GFP + rol-6(su1006)]	CGC	MAH240
C. elegans: AGD2213: uthIs439[hlh-17p:xbp-1s, myo-2p:tdTomato]; sqIs17[hlh-30p:hlh-30:GFP + rol-6(su10006)]	This study	AGD2213
C. elegans: AGD2788: sqIs17[hlh-30p:hlh-30:GFP + rol-6(su1006)]; unc-13(s69) I	This study	AGD2788
C. elegans: AGD2789: sqIs17[hlh-30p:hlh-30:GFP + rol-6(su1006)]; unc-31(e928) IV	This study	AGD2789
C. elegans: AGD2790: uthIs439[hlh-17p:xbp-1s, myo-2p:tdTomato]; sqIs17[hlh-30p:hlh-30:GFP + rol-6(su10006)]; unc-13(s69) I	This study	AGD2790
C. elegans: AGD2791: uthIs439[hlh-17p:xbp-1s, myo-2p:tdTomato]; sqIs17[hlh-30p:hlh-30:GFP + rol-6(su10006)]; unc-31(e928) IV	This study	AGD2791
C. elegans: AGD2669: uthEx935[hlh-17p:hlh-30(gDNA):tbb-2 3′UTR]	This study	AGD2669
C. elegans: AGD2769: uthEx935[hlh-17p:hlh-30(gDNA):tbb-2 3′UTR, unc-122p:RFP:unc-54 3′ UTR]; sqIs17[hlh-30p:hlh-30:GFP + rol-6(su1006)]	This study	AGD2769
C. elegans: AGD2671: uthEx937 [hlh-17p:hlh-30(gDNA):tbb-2 3′UTR]	This study	AGD2671

(*Continued on next page*)

Continued

REAGENT or RESOURCE	SOURCE	IDENTIFIER
C. elegans: AGD2348: hlh-30(tm1978) IV	CGC	AGD2348
C. elegans: AGD2491: uthIs440[hlh-17p:xbp-1s, myo-2p:tdTomato]; hlh-30(tm1978) IV	This study	AGD2491
C. elegans: SJ4005: zcls4[hsp-4p:GFP]V	CGC	SJ4005
C. elegans: uthIs439[hlh-17p:xbp-1s, myo-2p:tdTomato]; zcls4[hsp-4p:GFP]	Frakes et al. 2020[2]	AGD1566
C. elegans: AGD1415: pwIs23[vit-2:GFP]	Daniele et al. 2020[25]	AGD1415
C. elegans: AGD2274: uthIs439[hlh-17p:xbp-1s, myo-2p:tdTomato]; pwIs23[vit-2:GFP]	This study	AGD2274
C. elegans: GF80: dgEx80[pAMS66 vha-6p: Q44:YFP+rol-6(su1006)+pBluescriptII]	CGC	GF80
C. elegans: AGD2394: uthIs439[hlh-17p:xbp-1s, myo-2p:tdTomato]; dgEx80[pAMS66 vha-6p:Q44:YFP+rol-6(su1006)+pBluescriptII]	This study	AGD2394
C. elegans: MAH215: sqIs11 [lgg-1p:mCherry:GFP:lgg-1 + rol-6]	CGC	MAH215
C. elegans: AGD2212: uthIs439[hlh-17p:xbp-1s, myo-2p:tdTomato]; sqIs11[lgg-1p:mCherry:GFP:lgg-1 + rol-6]	This study	AGD2212
C. elegans: TJ356: zIs356[pGP30(daf-16p:daf-16a:GFP), pRF4(rol-6)]	CGC	TJ356
C. elegans: DA1116: eat-2(ad1116)II	CGC	DA1116
C. elegans: CB1372: daf-7(e1372)III	CGC	CB1372
C. elegans: AGD1873: uthIs439[hlh-17p:xbp-1s, myo-2p:tdTomato]; zIs356[pGP30(daf-16:daf-16a:GFP), pRF4(rol-6)]	This study	AGD1873
Software and algorithms		
GraphPad Prism	GraphPad	Version 9.0
COPAS Software	Union Biometrica, Inc.	N/A
ImageJ	NIH	N/A - download available from https://imagej.nih.gov/ij/
LAS-X	Leica Microsystems	N/A
ZEN Microscopy Software (Blue)	Zeiss	N/A

RESOURCE AVAILABILITY

Lead contact

Further information and requests for resources and reagents should be directed to and will be fulfilled by the lead contact, Dr. Andrew Dillin (dillin@berkeley.edu).

Materials availability

C. elegans lines generated in this study are available upon request.

Data and code availability

- The raw RNA-seq data have been deposited to Mendeley and are available as of the date of publication. Accession numbers are listed in the key resources table.
- There was no original code written for this publication.
- Any additional information required to reanalyze the data reported in this paper is available from the lead contact upon request.

EXPERIMENTAL MODEL AND SUBJECT DETAILS

C. elegans strains and details

Nematodes were maintained at 15°C or 20°C on standard nematode growth medium (NGM) agar plates seeded with *Escherichia coli* (*E. coli*) OP50. All experimentation was performed at 20°C on OP50 or HT115 *E. coli* K12 strain containing pL4440 empty vector control or expressing double-stranded RNA containing the sequence of the target gene for RNA interference (RNAi) experiments. RNAi strains were all isolated from Vidal or Ahringer libraries and sequence verified before use. For all experiments, animals are synchronized using a standard bleaching protocol where carcasses of reproductive animals are degraded using a bleach solution (1.8% sodium hypochlorite, 0.375 M KOH), followed by 5 washes with M9 buffer (22 mM KH_2PO_4 monobasic, 42.3 mM NA_2HPO_4, 85.6 mM NaCl, 1 mM $MgSO_4$) and eggs were then platted onto NGM plates spotted with OP50. Glial XBP-1s animals have a slight developmental delay, to account for this in glial XBP-1s were bleached 8 h before wild type animals for all experiments. All strains used in this study are listed in key resources table.

Transgenic worms (glial HLH-30) were synthesized by injecting N2 worms with plasmid pMM26 listed in key resources table at 50ng/ul with co-injection marker pEK2 (unc-122p:RFP (coelomocyte RFP)) at 50ng/ul and 100ng/ul of pD64 vehicle as filler DNA. *hlh-30* genomic DNA includes isoforms A, F, G, and H. Worms positive for *unc-122*p::RFP were selected for stable arrays.

METHOD DETAILS

Lifespan analysis

Lifespan analyses were performed on NGM plates at 20°C on HT115 *E. coli* strain expressing empty vector control or the designated double-stranded RNAi. Animals were age-synchronized by bleaching and plating on HT115 and grown from hatch to adulthood at 20°C unless otherwise stated. Bleach times were determined based on the developmental delay of strains so that all animals reach day 1 of adulthood at the same time. Adult animals were manually moved away from progeny onto fresh plates every day or every other day during reproduction. Animals were scored every 1–2 days for death or censored due to bagging, vulval explosions, or crawling off the plate. Lifespan analyses were blinded and performed a minimum of 3 times by at least 2 independent researchers. Representative data from one of the 3 trials were presented as a Kaplan-Meier curve. Prism 9 was used for statistical analyses, and p values were calculated using long-rank (Mantel-Cox) method.

Stereomicroscopy for fluorescent reporters

Animals were age-synchronized by bleaching, eggs were plated on NGM plates spotted with OP50 *E. coli* or HT115 *E. coli* expressing empty vector control or the designated double-stranded RNAi and grown to adulthood at 20°C. Animals were moved onto unspotted NGM plates on day 1 or day 2 of adulthood and anesthetized with 5 μL 100 mM sodium azide. Animals were imaged using a Leica M250FA automated fluorescent stereoscope equipped with a Hamamatsu ORCA-ER camera, standard GFP filter, and driven by LAS-X software. Each microscopy experiment was performed a minimum of 3 independent times.

BODIPY 493/503 staining

Animals were age-synchronized by bleaching, eggs were plated on NGM plates spotted with OP50 bacteria. At day 2 of adulthood, animals were washed off using M9, spun down at 1,000 RCF, and washed 3X with M9 in 15mL conical tubes. M9 was aspirated and replaced with 500 μL of 4% paraformaldehyde. Animals were fixed for 15 min while rotating in the dark at 20°C. Animals were then frozen in liquid nitrogen and thawed in a 37°C water bath, followed by a wash with 1X PBS, spin down at 1,000 RCF, and repeated a total of 3 times. 10 μL of 1 mg/mL BODIPY 493/503 was diluted 1:1000 in 10mL of PBS. Animals then were put on a rotator at 20°C in the dark for 1 h. After incubation with BODIPY 493/503, animals were washed 3 times with 1X PBS and spun down at 1,000 RCF after each wash. 5 mL 1X PBS was placed into each tube and fixed animals were incubated overnight at 4°C in the dark. The next day animals were washed 3 times with 1X PBS and then run through the COPAS BioSorter for whole worm fluorescence quantification.

Imaging of HLH-30 nuclear translocation assay

Day 2 adult animals were anesthetized in 15 μL 100 mM sodium azide on microscope slides and covered with a coverslip fastened with nail polish. Worms were imaged using a Zeiss AxioObserver.Z1 microscope equipped with a Lumencor SOLA light engine and a ZEISS Axiocam 506 camera, driven by ZEISS ZEN Blue software using a 63x/1.4 Plan Apochromat objective. Images of the anterior 30% of the intestine were taken using a 63× objective/1.4 Plan Apochromat objective and standard GFP filter (ZEISS filter set 46 HE). To avoid potential translocation phenotypes caused by exposure to the mounting and imaging conditions, all scoring was conducted within 5 min after mounting.

Whole animal fluorescence quantification

For large-scale quantification of fluorescent and dyed animals, a Union Biometrica complex object parameter analysis sorter (COPAS) BioSorter was used to measure GFP fluorescence of individual worms for quantification. Animals were washed off NGM plates using M9 wash and run through the COPAS BioSorter using a 488nm light source. Total integrated GFP fluorescence was normalized to extinction (thickness) of each animal. Data was processed by censoring events that reached the maximum peak height for green or extinction values (PH Green and PH Ext = 65532) and censoring events <300 and >1000 time of flight (length) to remove progeny and greater than one worm per event. Values of green ≤10 were removed for strains with visible fluorescence (BODIPY 493/503, *dhs-3*p::*dhs-3*::GFP) as these

values are most likely air bubbles detected by the sorter. All data was normalized to the mean of fluorescent values of wild-type animals. Each data point represents an individual animal measurement. All experiments were performed a minimum of 3 independent times. Statistics were calculated using Prism 9 software.

Measurement of polyQ aggregates

Animals were age-synchronized by bleaching and adding eggs to NGM plates spotted with HT115 *E. coli* expressing empty vector control (pL4440) or the designated double-stranded RNAi and grown to adulthood at 20°C. Animals were moved at day 2 of adulthood to new NGM plates spotted with HT115 *E.coli* and away from their progeny. Fluorescent microscopy was performed on day 3 of adulthood. Images were blinded and YFP-positive puncta were counted per animal, for a minimum of 100 animals per condition. Fluorescent microscopy is representative of 3 independent experiments.

qPCR

Animals were grown on standard NGM plates spotted with OP50 from hatch at 20°C until day 1 of adulthood. Animals were collected by washing off with M9 buffer. M9 was subsequently aspirated and replaced with Trizol (Invitrogen). Animals were homogenized via a freeze-thaw process 3x with liquid nitrogen. Following the final freeze-thaw cycle, chloroform was added at a 1:5 volumetric ratio (chloroform:Trizol) for aqueous separation of RNA via centrifugation in heavy gel phase-lock tubes (VWR). Aqueous phase was transferred into isopropanol followed by RNA purification using a Qiagen RNeasy Mini Kit as per the manufacturer's instructions. 0.5–2 ng of purified RNA was used for cDNA synthesis using the Qiagen QuantiTect Reverse Transcriptase kit as per the manufacturer's instructions. qPCR analysis was performed using a general standard curve protocol using SYBR-green on an Applied Biosystems QuantStudio 384-well qPCR machine. Per sample, 3 biological replicates and 4 technical replicates per independent biological replicate were run.

For the tunicamycin qPCR experiment, animals were synchronized and grown to D1 of adulthood on EV RNAi plates. Animals were then treated with either 1% DMSO or tunicamycin (25 ng/μL), rotating at 20°C for 1 h in a 15 mL conical tube. After an hour of treatment, M9 was aspirated, and animals were washed 3X with M9 buffer.

RNA isolation, sequencing, and analysis

Animals were bleach synchronized and grown to day 2 of adulthood on large NGM plates spotted with 1mL of OP50. Around 1,000 animals per condition and replicate were collected by washing off with M9 buffer. Each condition had a total of 5 biological replicates. Animals were spun down at 1,000 RCF for 30 s, M9 removed, and washed again for a total of 3 washes. M9 was then replaced with 1 mL of Trizol and animals were subsequently frozen, via liquid nitrogen, and thawed, in a 37°C water bath, 3 times. After the final thaw, chloroform was added at a ratio of 1:5 (chloroform:trizol) for aqueous separation of RNA using heavy gel phase-lock tubes (VWR, 10847-802). Library preparation and RNA-sequencing was performed by Genewiz (Azenta Life Sciences). Library preparation was performed with Poly A selection and HiSeq xSequencing using NEBNext Ultra RNA Library Prep Kit for Illumina. Sequencing libraries were clustered onto 1 lane of a flow cell, loaded on Illumina HiSeq instrument (4000 or equivalent) and samples were sequenced using 2x150bp Paired End configuration. Base calling was conducted on HiSeq Control Software. For RNA-sequencing analysis, raw sequencing data were uploaded to the Galaxy project web platform, and the public server at usegalaxy.org was used to analyze the data.[77] Paired end reads were aligned using the Kallisto quant tool (Version 0.48.0) with WBcel235 as the reference genome. Fold changes and statistics were generated using the DESeq2 tool with Kallisto quant count files as the input. The fold change and adjusted-p values generated by the DESeq2 analysis were used to plot the data using GraphPad Prism 9.

Electron microscopy imaging and analysis

Whole animal samples were processed for transmission electron microscopy (TEM) as previously described.[35] Briefly, staged animals were subjected to high-pressure freezing (BAL-TEC HPM 010) and freeze-substituted with acetone/resin series (25%-50%-75%–100% resin). Resin-cured animals were sectioned into 70nm sections and imaged using a FEI Tecnai 12 transmission electron microscope on formvar-coated mesh grids.

TEM images were analyzed using ImageJ. Rough ER was determined as described[78]; the rough ER is decorated with ribosomes which are detected in the TEM images as black dots. Using the freehand selection tool, the area of rough ER cisternae was determined as the space between the black ribosome dots that outline the rough ER cisternae. The circularity index was calculated using the circularity measurement in ImageJ. The circularity index was determined using the following formula *circularity = 4pi(area/perimeter^2)*.

Airyscan microscopy

Live animals at their listed respective age were paralyzed in 15 μL sodium azide (100 mM) on microscope slides and covered with a coverslip fastened with nail polish. Fluorescent images were obtained with a Zeiss LSM900 Airyscan microscope. Images were quantified using ImageJ.

LysoTracker blue DND-22 staining

Animals were grown from hatch to day 2 of adulthood on OP50 *E. coli* seeded NGM plates and then moved to OP50 seeded plates containing 10 μM ThermoFisher scientific LysoTracker Blue DND-22 (Invitrogen) (1mM stock diluted 1:100) or an equivalent volume of M9 buffer for 2 h.

After 2 h worms were moved and placed on OP50 plates for 1 h. Worms were then imaged by AiryScan microscopy, using 10 animals per genotype and 3 independent biological replicates. Quantification was carried out using ImageJ.

Pharyngal pumping assay

Animals were grown to day 1 on NGM plates seeded with OP50 *E. coli*. Young adults (early day 1) were then transferred to a new NGM plate seeded with OP50 *E. coli* and allowed to crawl on the plate for 15 min. Pharyngeal pumping rate was determined by visual counting of the movement of the grinder under a dissecting microscope for a total of 60 s, counting for 10 s with a 10-s break in between.

Heat shock assay

Animals were grown to day 2 of adulthood on NGM plates spotted with OP50 *E. coli* and exposed to a heat shock for 3 h at 35°C. HLH-30:GFP nuclear localization in the intestine was scored immediately as described in the 'imaging of HLH-30 nuclear translocation assay' STAR methods section.

Tunicamycin assay

Animals were grown to day 1 of adulthood, washed with M9 buffer for a total of three times, and then treated with either tunicamycin (25 ng/μL) or DMSO (1%) diluted with M9 buffer in a 15 mL conical tube. Animals were left rotating at 20°C for 1 h in the dark. Animals were then washed 3 times with M9 buffer and plated on OP50 *E. coli* spotted NGM plates to recover and imaged 1 h afterward.

QUANTIFICATION AND STATISTICAL ANALYSIS

All statistical analyses are specifically described in figure legends and in the Experimental methods above. Sample sizes are reported in the figure legend where *n* = animals. GraphPad Prism software version 9.0.0 for Mac (GraphPad Software, San Diego, California USA, www.graphpad.com) was used for all statistical tests and graphical representations.